

Stress Distribution on Bridge Abutment due to Live Loads

Saranya S

A Dissertation Submitted to
Indian Institute of Technology Hyderabad
In Partial Fulfillment of the Requirements for
The Degree of Master of Technology



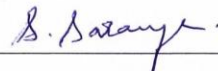
भारतीय प्रौद्योगिकी संस्थान हैदराबाद
Indian Institute of Technology Hyderabad

Department of Civil Engineering

June, 2013

Declaration

I declare that this written submission represents my ideas in my own words, and where others' ideas or words have been included, I have adequately cited and referenced the original sources. I also declare that I have adhered to all principles of academic honesty and integrity and have not misrepresented or fabricated or falsified any idea/data/fact/source in my submission. I understand that any violation of the above will be a cause for disciplinary action by the Institute and can also evoke penal action from the sources that have thus not been properly cited, or from whom proper permission has not been taken when needed.



(Signature)

S.Saranya

CE11M09

Approval Sheet

This thesis entitled 'Stress Distribution on Bridge Abutment due to Live Loads' by Saranya S is approved for the degree of Master of Technology from IIT Hyderabad.



Dr. B. Umashankar

Assistant professor

Department of Civil Engineering

Indian Institute of Technology Hyderabad

Advisor



Dr. K. B. V. N. Phanindra

Assistant Professor

Department of Civil Engineering

Indian Institute of Technology Hyderabad

Examiner



Dr. Raja Banerjee

Assistant Professor

Department of Mechanical Engineering

Indian Institute of Technology Hyderabad

Examiner

Acknowledgements

My sincere gratitude to my advisor Dr.B.Umashankar for his continuous support, help and motivation. I would like to thank all the faculty members of Civil Engineering Department.

I am grateful to my family members, Rubesh and Uma Maheshwari, for their valuable support.

My heartfelt thanks to my friends Sushmita, to my roomie Aiswarya, Kavita, Hari Prasad, Mouli, Deepti, Aranya, Sairam, and my juniors Preethi, Rajashekhar, Natasha, Akhila, Bhargav and my classmates Roji, Faby, Bhagath, Suraj and Rajashekar for being supportive all through the days.

Dedicated to

My Dad and Mom

Abstract

Stress distribution on the bridge abutment plays a key role in the design of bridge abutments. Lateral stress on the abutment will be due to backfill and live loads (wheel loads). Lateral stress due to backfill can be determined by classical earth pressure theories that are well documented in the literature. However, the effect of lateral stress distribution due to live loads/wheel loads are typically assumed as an equivalent uniformly distributed load of additional height of surcharge of backfill over the surface of the backfill. IRC recommendation of 1.2m height of surcharge is based on engineering judgment and experience. This study aims to predict the lateral stress on bridge abutment more closely to the actual values. A model was developed using finite element package PLAXIS and the lateral stress distribution on abutment for various lanes are obtained. In the present study, abutment-soil system was modeled considering two cases- (a) two-layered system with a granular base layer/approach slab resting on the embankment fill material, and (b) three-layered system with an approach slab over the granular base layer resting on the embankment fill material. The equivalent height of surcharge is proposed for various moduli ratio of the pavement layers and for different lane widths (corresponding to one, two, three, four and five lanes). It is determined that the equivalent height of surcharge for case(a) two-layered system is in the range of 0.7m-1.3m and for case(b) three-layered system with an approach slab is in the range of 0.5m-0.9m.

Contents

Declaration.....	Error! Bookmark not defined.
Approval Sheet	Error! Bookmark not defined.
Acknowledgements.....	iv
Abstract.....	vi
1 Introduction.....	10
1.1 Overview.....	10
1.2 Objectives of the study	11
1.3 Organization of the study.....	11
2 Literature Review	12
2.1 Introduction.....	12
2.2 Failure modes in Abutment	12
2.3 Literature review on earth stress due to surface loads	13
2.3.1 Parallel Line Load of Infinite Length.....	14
2.4 Literature review on lateral stress on abutment due to live loads.....	16
2.5 Literature review on Approach Slab.....	16
3 Modeling Abutment-Soil System in PLAXIS 2D.....	18
3.1 Introduction.....	18
3.2 Finite element model	18
3.3 Finite elements.....	19
3.4 Interface elements.....	19
3.5 Boundary Conditions	20
3.6 Meshing	20
3.7 Validation studies	21
3.7.1 Mirror image effect	21
3.7.2 Homogeneous medium.....	22
3.7.3 Two-layered system	23
3.7.4 Three-layered system	24
3.8 Abutment-soil System	25
3.8.1 Effect of top layer thickness	25
3.8.1.1. Vertical Stress.....	25

3.8.1.2.	Lateral Stress	26
3.8.1.3.	Settlement Profile	27
3.8.2	Effect of Moduli ratio.....	28
3.8.2.1.	Vertical stress	28
3.8.2.2.	Lateral stress	28
3.8.2.3.	Settlement Profile	29
4	Modeling Abutment-Soil System in PLAXIS 3D	30
4.1	Introduction.....	30
4.2	Problem Definition and Objectives of the Study	31
4.3	Finite element Model.....	32
4.3.1	Finite elements	33
4.3.2	Plate elements.....	33
4.3.3	Interface elements.....	33
4.3.4	Meshing.....	34
4.4	Validation studies	35
4.5	Methodology.....	35
4.6	Equivalent live load surcharge.....	36
4.6.1	Equivalent Bending moment and Force methods.....	36
4.7	Loading condition as per IRC 6-2000.....	38
4.7.1	Class AA Loading	38
4.7.2	Class A Loading	39
4.8	Lateral stress distribution considering Two-layered system.....	41
4.8.1	Two Lanes	41
4.8.1.1.	Variation of lateral stress with depth for $E_1/E_2=4.0$ and 8.0	42
4.8.1.2.	Variation of lateral stress with carriageway width for $E_1/E_2=4.0$ and 8.0	43
4.8.1.3.	Variation of lateral stress with depth for $E_1/E_2=4.0$	44
4.8.2	One Lane	45
4.8.2.1.	Variation of lateral stress with depth for $E_1/E_2=4.0$ and 8.0	45
4.8.2.2.	Variation of lateral stress with carriageway width for $E_1/E_2=4.0$ and 8.0	46
4.8.3	Three Lanes	47
4.8.3.1.	Variation of lateral stress with depth for $E_1/E_2=4.0$ and 8.0	47
4.8.3.2.	Variation of lateral stress with carriageway width for	

E ₁ /E ₂ =4.0 and 8.0.....	48
4.8.3.3. Variation of lateral stress with depth for E ₁ /E ₂ =4.0.....	49
4.8.4 Four Lanes.....	50
4.8.4.1. Variation of lateral stress with depth for E ₁ /E ₂ =4.0 and 8.0.....	50
4.8.4.2. Variation of lateral stress with carriageway width for E ₁ /E ₂ =4.0 and 8.0.....	50
4.8.4.3. Variation of lateral stress with depth for E ₁ /E ₂ =4.0.....	52
4.8.5 Five Lane.....	52
4.8.5.1. Variation of lateral stress with depth for E ₁ /E ₂ =4.0 and 8.0.....	52
4.8.5.2. Variation of lateral stress with carriageway width for E ₁ /E ₂ =4.0 and 8.0.....	53
4.8.5.3. Variation of lateral stress with depth for E ₁ /E ₂ =4.0.....	54
4.9 Lateral stress distribution considering Three-layered system.....	55
4.9.1 Single lane.....	55
4.9.1.1. Comparison of Variation of lateral stress with depth for E ₁ /E ₂ =8.0.....	56
4.9.1.2. Variation of lateral stress with carriageway width for E ₁ /E ₂ =8.0.....	56
4.9.2 Two lanes.....	57
4.9.2.1. Comparison of Variation of lateral stress with depth for E ₁ /E ₂ =8.0.....	57
4.9.2.2. Variation of lateral stress with carriageway width for E ₁ /E ₂ =8.0.....	57
4.9.3 Three lanes.....	58
4.9.4 Four lanes.....	59
4.9.5 Five lanes.....	59
5 Equivalent surcharge for live loads on Abutments	61
5.1 Introduction.....	61
5.2 Two-Layered System-Model I.....	61
5.3 Calculation of Equivalent height of surcharge.....	61
5.3.1 Equivalent bending moment method.....	62
5.3.2 Equivalent force method.....	62
5.4 Critical position of the vehicle.....	63
5.5 Effect of Moduli Ratio.....	64
5.6 Values of equivalent height.....	65
5.7 Three-Layered System-Model-II.....	66
6 Conclusions.....	68
References.....	71

Chapter 1

Introduction

1.1 Overview

Abutments are retaining structures provided at the ends of the bridge to retain the embankment fill as well as to transfer the vertical and horizontal loads from the superstructure to the foundation [14], as illustrated in Figure 1.1. Abutments also support the approach slabs. Typically, abutments are designed similar to retaining walls. Abutments are designed to withstand the self-weight from the superstructure, the live load surcharge, and the lateral loads due to backfill. Foundation of abutments must be designed to prevent differential settlements and excessive lateral movements. The Classical earth pressure theories available in the literature to predict the lateral earth pressure on the walls are either empirical or analytical in nature. Lateral earth pressure on walls backfilled with cohesionless soil can be designed using effective stresses in accordance with Rankine's and Coulomb's earth pressure theories. Walls backfilled with cohesive soils shall be designed using equivalent fluid pressure method, empirical charts are proposed by Terzaghi and Peck (1948) to predict the lateral pressure. In traditional methods, the lateral earth pressure on a retaining structure that is due to live load surcharge is estimated by replacing with a uniformly distributed load over the entire backfill. Experimental studies has been carried out Spangler (1936) [8] to calculate the lateral earth pressure on retaining wall due to concentrated load applied at the surface of the homogeneous backfill, uniformly distributed line or strip loads parallel to the wall, and spread footing on the surface of the backfill. In traditional methods, the lateral earth pressure on a retaining structure due to live load surcharge is estimated by replacing it with a uniformly distributed surcharge load acting on the backfill surface. In present practice, the abutments, return walls, retaining walls of road bridges are designed for earth pressure loading as specified in clause 214 of IRC: 6-2010. For calculation of live load surcharge, the equivalent height of soil for vehicular loading is proposed to be taken as 0.9m as against 1.2m in earlier version. The provision is in line with AASHTO LRFD 2007 clause no. 3.11.6.4. However, IRC loading conditions are different from AASHTO specifications, and hence the equivalent height of soil for live load surcharge corresponding to IRC loading conditions needs to be determined.

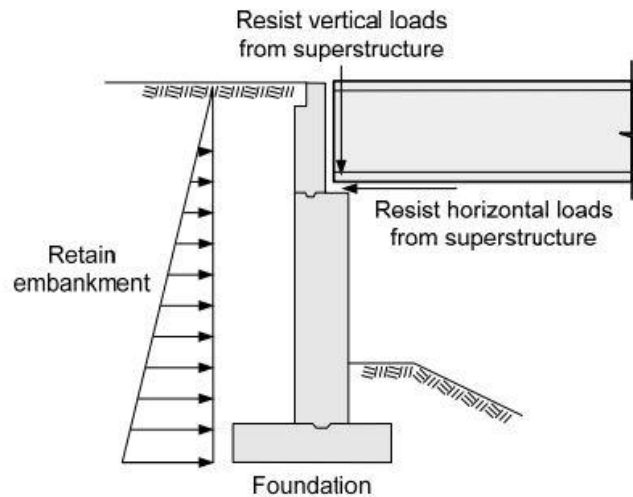


Figure 1.1: Primary Function of Bridge abutment

In addition, the presence of a stiffer layer (due to approach slab or granular layer or both) on top of embankment fill will alter the lateral stress distribution on the abutments. Hence, the equivalent height of surcharge should account for layered-soil system.

1.2 Objectives of the study

Objectives of the present study are the following:

- To perform a Finite element analysis (both 2D and 3D) to study the effects of stiffer layer over the embankment fill material on the stress distribution on abutments in a two-layered system.
- To obtain the equivalent height of surcharge for different lane widths (one, two, three, four and five) and for various moduli ratio of top and bottom layers in a two-layered system.

1.3 Organization of the study

Chapter 2 deals with the literature review on the studies available to calculate the lateral stress distribution on abutment or retaining walls. In this Chapter, the different approaches followed to determine the lateral stress distribution on the abutment as per the Standard codes of practice is also provided. Chapter 3 provides the modeling background in PLAXIS 2D of the abutment-soil system. In addition, the validation studies conducted with the various available elastic solutions is presented. Discussion about the 2D finite element model and the effects of moduli ratio and the thickness-to-radius ratios is also provided in this Chapter. Chapter 4 discusses the basic ideas on modeling in 3D and the importance of 3D modeling in such problems, followed by the lateral stress distribution for different lane widths and for different moduli ratios. Chapter 5 comprises of the results and discussion on the equivalent height of surcharge, calculated from the studies conducted for different lane widths.

Chapter 2

Literature Review

2.1 Introduction

Abutments are components of a bridge which provides vertical support to the bridge superstructure at the bridge ends, connects the bridge with the approach roadway, and retains the roadway base materials from the bridge spans. Abutments are subjected to lateral earth stress due to adjacent backfilled earth mass and live load acting on the backfill. Classical earth pressure theories (for example, Rankine's, Coulomb's, Terzaghi's, etc.) to calculate the lateral earth stress due to backfill only is well documented in the literature. Some of them are elastic solutions proposed by Boussinesq, Spangler, Terzaghi, and Mindlin. However, limited studies are available on in the literature to predict the lateral earth stress on bridge abutment due to live wheel loads. This Chapter provides a review on the available solutions and some of the approaches presently followed to predict the lateral earth stress on the abutment wall.

2.2 Failure modes in Abutment

Abutments are subjected to various limit states or type of failures.

- Sliding failure will occur when the lateral earth stress exerted on the abutment exceeds the frictional sliding capacity of the foundations.
- Bearing capacity failure will result if the bearing stress is larger than the capacity of the foundation soil or rock.
- Deep seated failure may become imminent when slip develops along a surface within the foundation soil.

To evaluate the safety of abutment, the lateral earth stress due to all the loads acting on the structure should be predicted accurately. In this study, focus is on calculation of the lateral earth stress due to live wheel loads.

2.3 Literature review on earth stress due to surface loads

Many studies were proposed to calculate the effect of surcharge loads on the backfill surface. Even though the backfill is not an elastic material, the elastic solution originally proposed by Boussinesq (1876) has been commonly adopted to estimate the earth stress due to surface loads. According to Boussinesq's solution, the surface of the soil mass is assumed to be semi-infinite and homogenous. IOWA engineering experiment station conducted research between 1931-to-1941 to determine the lateral earth stress on a wall due to (i) Concentrated load applied at the surface of the backfill, (ii) Uniformly distributed line or strip loads parallel to the wall, and (iii) Spread footing on the surface of the backfill. Spangler (1936) and Spangler and Mickel (1956) conducted experiments to measure the stresses behind a wall due to point loads, line loads, and area loads. Experiments were performed on a rigid retaining wall of 1.83m (6 feet) height above the base. Backfill consisted of pit run gravelly sand with about 40% gravel, 48% sand, 8% silt and 4% of 5 μ m size clay. The liquid limit and plasticity index were 17% and 4%, respectively. Backfill was placed without special compaction. Loads were applied using heavily loaded trucks. He found that the observed stresses were considerably higher than that obtained from the Boussinesq solution. Empirical equations proposed by Spangler and Boussinesq are given in Equations [2.1] and [2.2], respectively.

$$\frac{\sigma_h H^2}{P} = \left(\frac{x}{z}\right)^2 \left(\frac{H}{z}\right)^2 \frac{1}{\left(\left(\frac{x}{z}\right)^2 + 1\right)^{5/2}} \quad (2.1)$$

$$\frac{\sigma_h H^2}{P} = \frac{3}{2\pi} \left(\frac{x}{z}\right)^2 \left(\frac{H}{z}\right)^2 \frac{1}{\left(\left(\frac{x}{z}\right)^2 + 1\right)^{5/2}} \quad (2.2)$$

where,

P= Concentrated Load

x = Distance from the wall to the concentrated load

z = Depth from the surface

H= height of the retaining wall

Comparing the lateral stress calculated using Spangler and Mickle (1956), and Boussinesq (1876) equations, the variation of lateral stress with depth were found to be similar.

Mindlin (1936) pointed out that a perfectly rigid wall would have lateral stresses exactly double those of a perfectly flexible wall, and the lateral stress measured by Spangler during the experiments agreed with Boussinesq solution but the magnitudes were about twice of the values calculated by Boussinesq equation in semi-infinite medium with backfill material of Poisson ratio's ration equal to 0.5.

Terzaghi (1956) proposed empirical equations and he indicated that the values form the ‘Upper limiting Values’ for lateral stresses. The proposed equations are given for $z/H \leq 0.4$ and for $z/H > 0.4$ (Equations [2.3] and [2.4]).

$$\frac{\sigma_h H^2}{P} = \frac{0.28 \left(\frac{z}{H} \right)^2}{\left(0.16 + \left(\frac{z}{H} \right)^2 \right)^3} \quad \text{for } \frac{z}{H} \leq 0.4 \quad (2.3)$$

$$\frac{\sigma_h H^2}{P} = \frac{1.77 \left(\frac{z}{H} \right)^2 \left(\frac{x}{H} \right)^2}{\left(\left(\frac{x}{H} \right)^2 + \left(\frac{z}{H} \right)^2 \right)^3} \quad \text{for } \frac{z}{H} > 0.4 \quad (2.4)$$

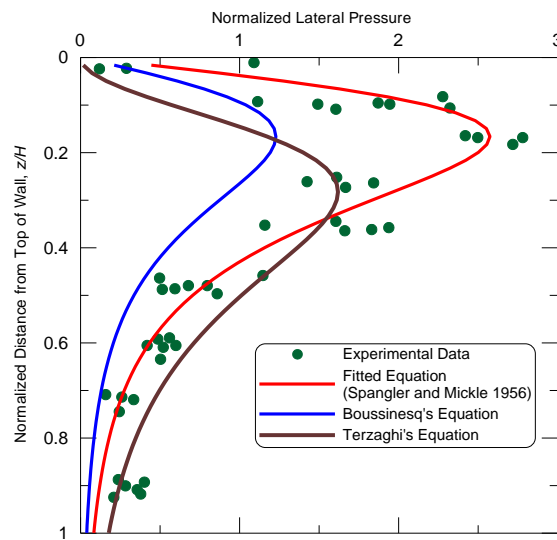


Figure 2.1: Lateral stress vs. depth for $P= 4.45 \text{ kN}$, $x/H=0.33$

Figure 2.1 shows the comparison of lateral stresses computed using Terzaghi’s (1956), Spangler and Mickle’s (1936), and Boussinesq’s (1876) equations.

2.3.1 Parallel Line Load of Infinite Length

Spangler (1956) proposed solutions for various types of loading. If a line load (such as a very long footing) is applied parallel to the wall it may be considered to extend from any point on the wall from $+\infty$ to $-\infty$, as illustrated in Figure 2.2. For this case, the lateral stress can be found by the relationship given in Equation [2.5].

$$\sigma_h = 1.33 P_L \frac{x^2 z}{R^4} \quad (2.5)$$

where,

P_L = Load per unit length

x = Distance from the wall to the line load as illustrated in Figure 2.2

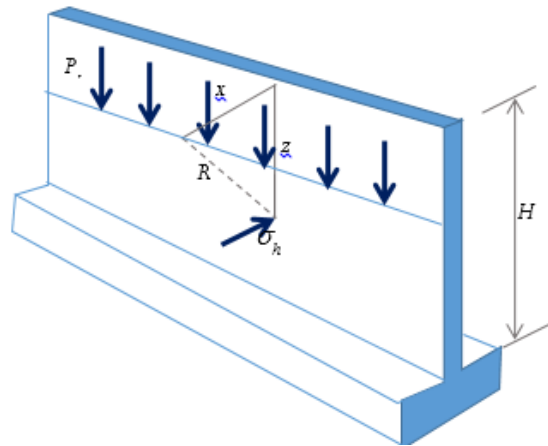


Figure 2.2: Line load of infinite length parallel to the wall

Uniform surcharge load applied on the ground surface over a large area causes a uniform increase in the vertical stress of the same amount. In such cases, the lateral stress can be computed by treating the surcharge as if it were backfill and multiplying the vertical stress at any depth by the appropriate earth pressure coefficient.

Davis and Poulos (1974) provided methods to estimate the stress due to various surface loads, such as area load and strip load. Their methods were primarily based on the classical solutions proposed by Boussinesq.

Pavement structures are layered systems with top layers consisting of stiffer material and hence cannot be treated as a homogeneous mass. Burmister's (1943) layered theory is more appropriate to calculate the stresses within the pavement layers. Burmister first developed the solution using strain continuity equations for two-layered system and then extended it to a three-layered system. Burmister's solution is based on the assumptions that each layer is homogeneous and isotropic, the material is weightless and infinite in areal extent. Each layer has a finite thickness, except the bottom layer which extends semi-infinitely in the depth direction. He proposed charts that show the effect of the stiff pavement layer on the distribution of vertical stresses under the center of a circular loaded area for various moduli ratio of the pavement layers. Influence chart was proposed to determine the vertical stress at the pavement-subgrade interface.

Jones et al. (1962) developed stress factors for three-layered system to determine the vertical and horizontal stresses at the interface of each layer. He tabulated the stress factors for varying thickness of each layer and the modulus of each layer. The limitation about this method is interpolation may be required if the required parameters are different from the tabulated parameters.

Peattie (1962) plotted Jones' table in graphical forms. The chart has the advantage that the interpolation for different parameter can be easily done.

2.4 Literature review on lateral stress on abutment due to live loads

Prasad et al. (2012) proposed a simple approach to analyze the stress in the two layered soil medium which uses the classical Boussinesq's equation coupled with equivalent thickness concept proposed by Palmer and Barber (1940). The study showed that E_1/E_2 ratios have pronounced effect in dissipating the stresses and E_1/E_2 ratio equal to 10 seems to have optimum effect on stress dissipation. If the replacement of the top layer by a stiffer layer is effected up to 0.25 times the width of the footing, the stress dissipation with increase in stress ratios is quite high.

2.5 Literature review on Approach Slab

Zahw et al. (2012) investigation suggests new models for designing and construction of the pavement approach slabs that minimizes problems such as settlement of the embankment under approach slab, and rutting and cracking that occurs at the top of asphalt layer.

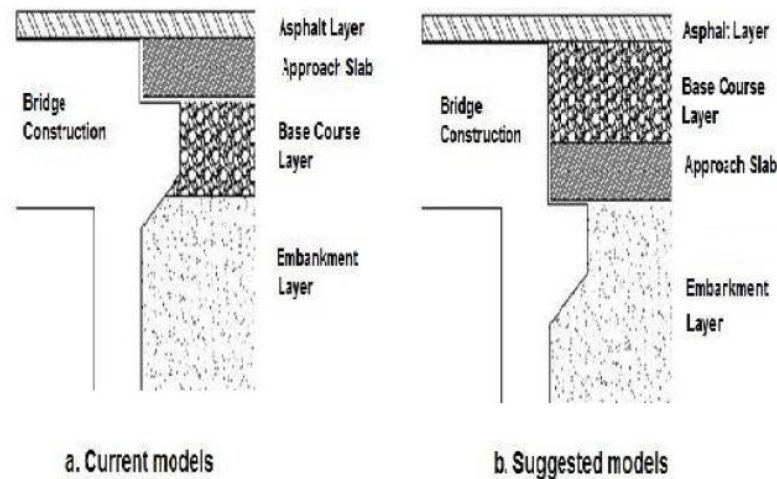


Figure 2.3: Current and suggested models and their layer configuration (Zahw et al. (2012))

The layer configuration of the pavement approach slab has a direct effect on the settlement that occurs at the top of embankment or base course beneath the approach slab. When the approach slab is kept below the base course layers, the settlements are found to be lower than that for the case when the approach slab is placed above the base course layers (refer Figure 2.3). In addition, the increase in the approach slab/ base course layer thickness improves the pavement performance by reducing the settlements. The vertical stresses values below the approach slab of the suggested model are less than those the values of the current models by about 82% when 254mm thick approach slab is used.

Shave et al. (2010) has developed a model to represent the horizontal load surcharges on abutment walls, wing walls and other retaining structures due to traffic loads. These models have been developed based on analysis of global and local effects of the traffic loads in the UK National Annex to BS EN1991-2. The standard approach followed to design highway structures for traffic surcharge loads in the UK is in accordance with the requirements of *Design Manual for Roads and Bridges* (BD 37/01), which specifies a vertical live load surcharge equivalent to 20kN/m^2 . This vertical load is

typically converted into a lateral earth stress on design using an appropriate earth pressure coefficient. An equivalent surcharge model was developed to analyze the vehicle loading specified in BS EN1991-2 using analytical methods such as Coulomb wedge analysis, Rankine with vertical Boussinesq and CIRIA C580 method (2003) (based on *Report on Embedded retaining walls-Guidance for economic design*). The proposed model consists of a horizontal knife edged load at the top of the wall of $660k_d kN$ combined with a horizontal uniformly distributed load with a magnitude of $20k_d kPa$ for normal loading, where k_d is the design value, equal to k_a for flexible walls and k_o for rigid walls. The developed surcharge models have been incorporated into PD 6694-1 in the manual of *Recommendations for the design of structures subject to traffic loading (BS EN 1997-1: 2004)*.

Kim et al. (2002) provided an analytical approach to estimate the earth stress due to live loads. Calibration procedure for the traditional method is also recommended in this paper. The original recommendation was made several decades ago on lateral earth stress due to live load surcharge in the design of abutments and retaining walls. They provided a rational method to determine the equivalent height of the backfill due to heavier highway loads that are specified in the design codes. However, the placement of a uniform load over an infinite area produces a constant lateral stress throughout the wall height. Available elastic solutions for strip load and an area load acting on the surface was used to obtain the actual lateral earth stress produced by AASHTO vehicular loading. Based on the elastic theory, the equivalent height of soil was generated for the live load model as given in the AASHTO LRFD specifications. Shorter walls must have a larger equivalent surcharge height h_{eq} than that of taller walls. Values are recommended based on the vehicle location from the wall. These values are applicable to rigid and flexible walls.

The only evidence found in the literature to support the selection of 600mm layer of additional backfill height for AASHTO standards is the following statement by Peck et al.(1974), 'Usually the wheel loads are assumed to be equivalent to a uniformly distributed load often taken as 11.5 kPa (240psf) for H-10 highway loading.' This recommendation was made several decades ago and appears to be based simply on engineering judgment and experience.

As per clause 217.1 in IRC 6(2000), all the abutments and return walls shall be designed for a live load surcharge equivalent to 1.2m earth fill.

Chapter 3

Modeling Abutment-Soil System in PLAXIS 2D

3.1 Introduction

When the geometry, loading and boundary conditions are simple, the analytical elastic solutions are available to calculate the stresses and displacements within the material. However, analysis of complex geometry, loading and boundary conditions are only possible with the help of approximate numerical solutions. Among the various numerical solutions available, Finite element analysis is a widely used technique. The basic idea of finite element method is to divide the structure or region into large number of finite elements which are interconnected by nodes, analyze each element in local co-ordinate system and combine the results in global co-ordinate system to get the unknown variable for the entire system. Dividing the whole domain into smaller elements has several advantages - accurate representation of geometry, inclusion of dissimilar material properties, easy representation of the total solution and ability to capture local effects.

3.2 Finite element model

A two-dimensional finite element analysis was performed using PLAXIS 2D. One dimension is very large compared to others and hence the principal strain in the longest dimension is constrained and assumed to be zero yielding plane strain condition. In the two dimensional stress analysis, abutment-soil system has been considered as plane strain condition. The width of the loading is denoted by 'b' as shown in Figure 3.1. The distance between the right boundary and center of loading is taken to be at a distance of 16 times the width of loading. This boundary distance is found to eliminate boundary effects on calculated stresses or displacements. Similarly for all cases considered in this study, the bottom boundary is also taken 16 times the width of the load from the loading surface.

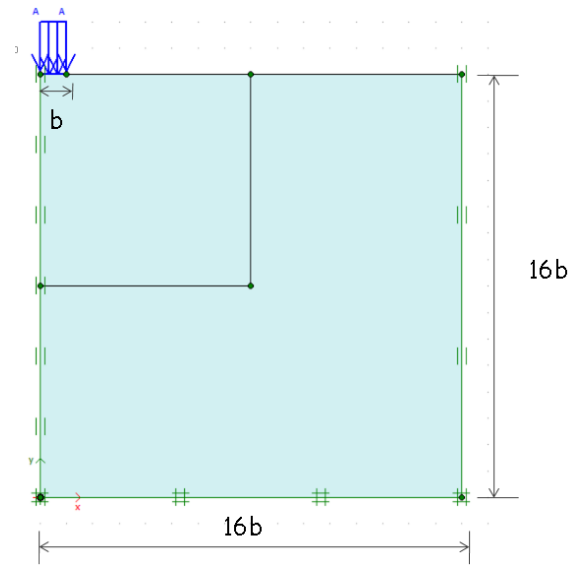


Figure 3.1: Model of Abutment-soil system in PLAXIS 2D

3.3 Finite elements

15-noded-triangular elements are used to model the soil layers and other volume clusters. The 15-node triangle is very accurate element that can produce high quality stress results for difficult problems, hence this can be used for the analysis. This type of element involves fourth order interpolation for displacements, and numerical integration involves twelve Gauss points (also called as stress points). Position of nodes and the stress points in 15-node triangular soil element are shown in Figure 3.2.

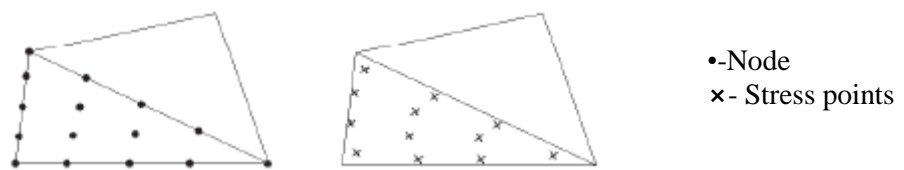


Figure 3.2: Position of Nodes and Stress points in the element

3.4 Interface elements

Interface elements can be modeled to enable full interaction between the structural objects (walls, plates, geogrids, etc.,) and the surrounding soil. A typical application would be in a region which is intermediate between smooth and fully rough. The roughness of the interaction is modeled by choosing a suitable value for the strength reduction factor in the interface. Interface elements have zero thickness in the finite element formulation. Interfaces are composed of interface elements. When using 15-node soil elements, the corresponding interface elements are defined by five pairs of nodes and five stress points. Corners in stiff structures and an abrupt change in boundary condition may lead

to peaks in stresses and strains. Volume elements are not capable of reproducing these sharp peaks and will, as a result, produce non-physical stress oscillations. The problem can be solved by the use of interface elements as shown in Figure. 3.3.

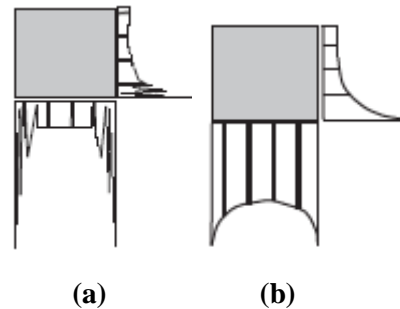


Figure 3.3: Improved results of stress oscillation using interface elements- (a) without interface and (b) with interface

Interface elements are extended below or around the corner of the structures used in the analysis meant to avoid stress oscillations, these are not meant to model soil- structure interaction, but it is just to allow for sufficient flexibility. The strength reduction in the interfaces should not be considered in such cases.

3.5 Boundary Conditions

Boundary conditions can be applied using fixity options. Fixities are defined as prescribed displacements at geometry line which is equal to zero. Fixity can be provided by selecting the geometry line and applying either horizontal ($u_x=0$), vertical ($u_y=0$), and total fixity ($u_x=u_y=0$) or by selecting the geometry line and applying a standard fixity condition available in PLAXIS. By selecting standard fixity, PLAXIS automatically implies a set of the following boundary conditions:

- Vertical geometry lines for which the x - coordinate is equal to the lowest or highest x -coordinate (right and left boundaries of the model) in the model obtain a horizontal fixity ($u_x=0$).
- Horizontal geometry lines for which the y -coordinate is equal to the lowest y -coordinate (bottom boundary) in the model obtain a full fixity ($u_x= u_y =0$).

3.6 Meshing

When the geometry model is fully defined and material properties are assigned to all the clusters and structural objects, the geometry has to be divided into finite elements in order to perform the finite element calculations. A composition of finite elements are called as mesh. The generation of mesh is based on robust triangulation procedures, which results in ‘unstructured meshes’. These meshes may look disorderly, but the numerical performance of such meshes are usually better than the structured/regular meshes. PLAXIS 2D allows fully automatic finite element mesh generation, which may not be accurate enough to produce accurate numerical results. Global coarseness is distinct in five levels: *Very coarse, coarse, medium, fine, and very fine*. The average element size and the number of generated triangular elements depends on this global coarseness.

In areas where large stress concentrations or large deformation gradients are expected, it is desirable to have a fine or very fine finite element mesh, whereas other parts of the geometry might not require a fine mesh. Such a situation often occurs when the geometry model includes edges or corners or structural objects. This can be performed by local coarseness parameters in addition to the global coarseness parameter. These parameters give an indication of the relative element size with respect to the average element size as determined by the global coarseness parameter.

3.7 Validation studies

3.7.1 Mirror image effect

When the surface loading is not uniform, or does not act over a large area, more complex calculations are needed to estimate the magnitude of induced lateral stresses. Although exact solutions to this problem have not been developed, a simple approximation has been found in the literature that is accurate enough for the practical purposes. Boussinesq developed expressions for the stresses induced within an elastic mass by a point load acting on the surface. Boussinesq's solution can be used to develop an expression for the lateral stress on a wall due to point load on the surface considering the following two assumptions

- The wall does not move, and
- The wall is perfectly smooth, i.e., there is no shear stress between the wall and the soil

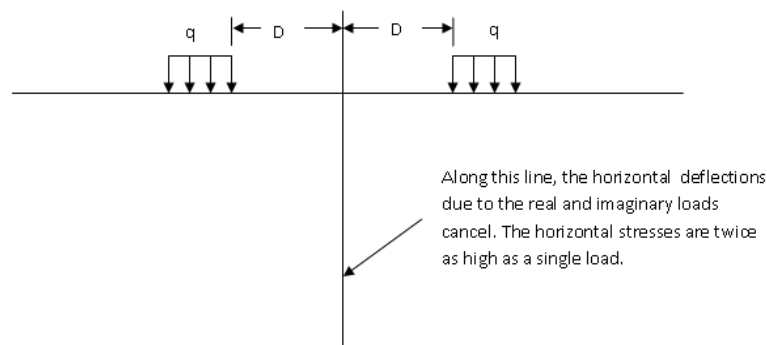


Figure 3.4: Mirror Image effect

Under these conditions the stresses developed on the wall would be the same as the stresses induced in an elastic half space by two loads of equal magnitude as shown in Figure. 3.4. The second fictitious load would cause equal and opposite normal displacements on a plane midway between it and the real load, thus enforcing the zero horizontal displacement boundary condition at the wall. The lateral stresses on a non-yielding wall can be treated to be equivalent to load applied on the boundary of the soil mass and a fictitious load that is mirror-image of this load about the wall face. Thus, the lateral stress on the wall are twice as large as the lateral stress induced in an elastic half-space due to a single point load

3.7.2 Homogeneous medium

To obtain the lateral stress on a non-yielding wall, lateral stresses obtained using Boussinesq's solution is doubled to account for zero displacement boundary condition normal to the wall by application of two symmetrical loads as shown in Figure 3.5. Spangler (1938) and Terzaghi (1954) performed experiments and compared the measured and calculated stresses on the wall due to point loads. These experiments confirmed the fact that doubling the free field stress provides a good approximation to the measured lateral earth stress on the wall.

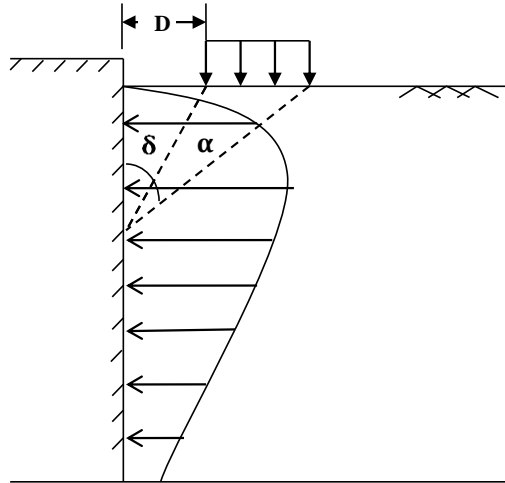


Figure 3.5: Lateral earth stresses on the wall due to uniform strip load

For an infinitely long strip load, Scott (1963) developed the following equations [Equations (1) and (2)] to calculate lateral and vertical stress increments, Δp_h and Δp_v , on the wall due to a vertically loaded strip of infinite length oriented parallel to a wall.

$$\Delta p_h = \frac{2p}{\pi} [\alpha - \sin\alpha \cos(\alpha + 2\delta)] \quad (1)$$

$$\Delta p_v = \frac{2p}{\pi} [\alpha + \sin\alpha \cos(\alpha + 2\delta)] \quad (2)$$

The abument wall has been modelled in PLAXIS 2D, where fixed horizontal displacements are considered to represent the rigid wall. The distance between the wall and the edge of the load is denoted by D . Distribution of the vertical and the lateral stresses on the wall is calculated for various D values using equations proposed by Scott (1963). The results obtained from PLAXIS 2D compare well with the elastic solution proposed by Scott (Figures 3.6 and 3.7).

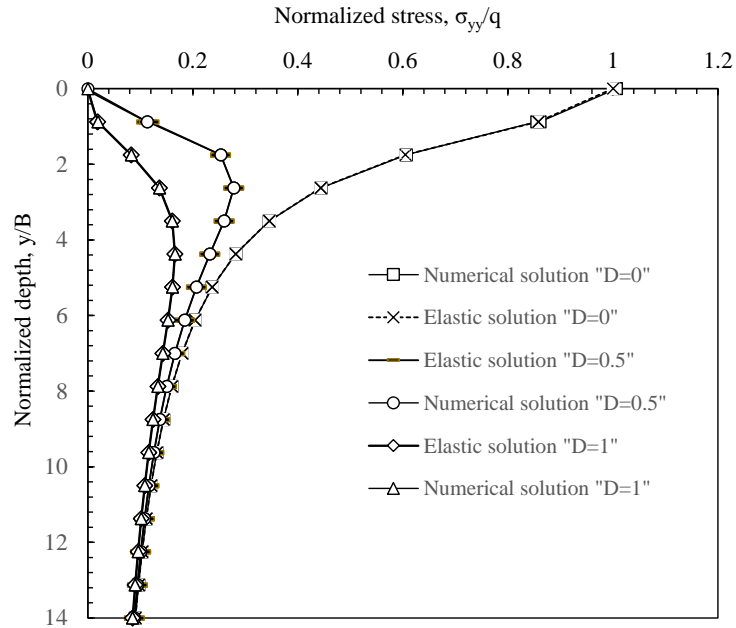


Figure 3.6: Vertical stress due to strip load

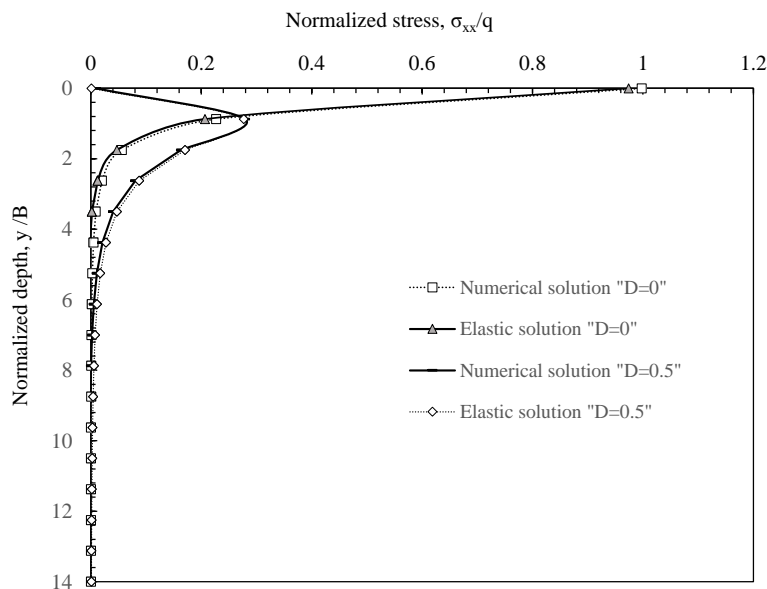


Figure 3.7: Lateral stress due to strip load

3.7.3 Two-layered system

In practice, pavements are layered systems with relatively stiffer materials on top and cannot be represented by a homogeneous mass. To study the effect of the stiffer pavement layer, a two-layered system has been modelled for finding the stress distribution on the bridge abutment. Burmister (1943) worked on such problems involving two-layered systems. The radius of the circular load is represented by 'a' and the elastic properties of the top and bottom layers are E_1 , ν_1 and E_2 , ν_2 , respectively. The stresses in the two-layered system depends on the modulus ratio E_1/E_2 and the thickness-to-radius ratio, h_1/a . The chart is applicable for the case when the thickness h_1 of layer 1 (top layer) is equal to

the radius of the contact area, i.e., $h_1/a=1$. Poisson's ratio equal to 0.5 is assumed for all the layers. To validate the two-layered model developed in PLAXIS, the solution was compared with the elastic solution proposed by Burmister. Burmister (1943) first developed the solution for a two-layered system. Results from the finite element model are found to be in good agreement with the elastic solution by Burmister (Figure 3.8).

It can be seen that the vertical stresses decreases significantly with the increase in the modulus ratio. For a homogenous soil, the vertical stress is about 68% of the load applied at a surface for a depth equal to the radius of the load. For a stiff layer on the top, the vertical stress decreases significantly compared to the homogenous case. For example, the vertical stress becomes 40% of the applied load for $E_1/E_2=5$ at a depth equal to radius of the load.

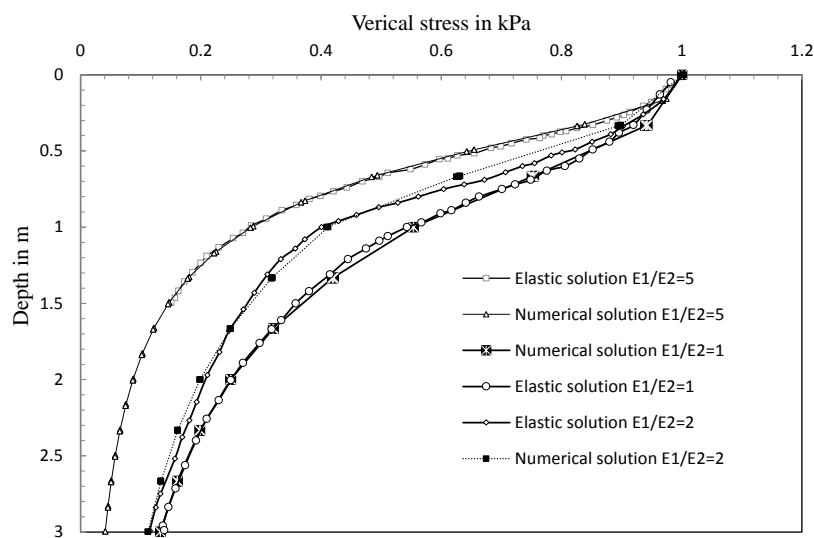


Figure 3.8: Stresses in two layered system

3.7.4 Three-layered system

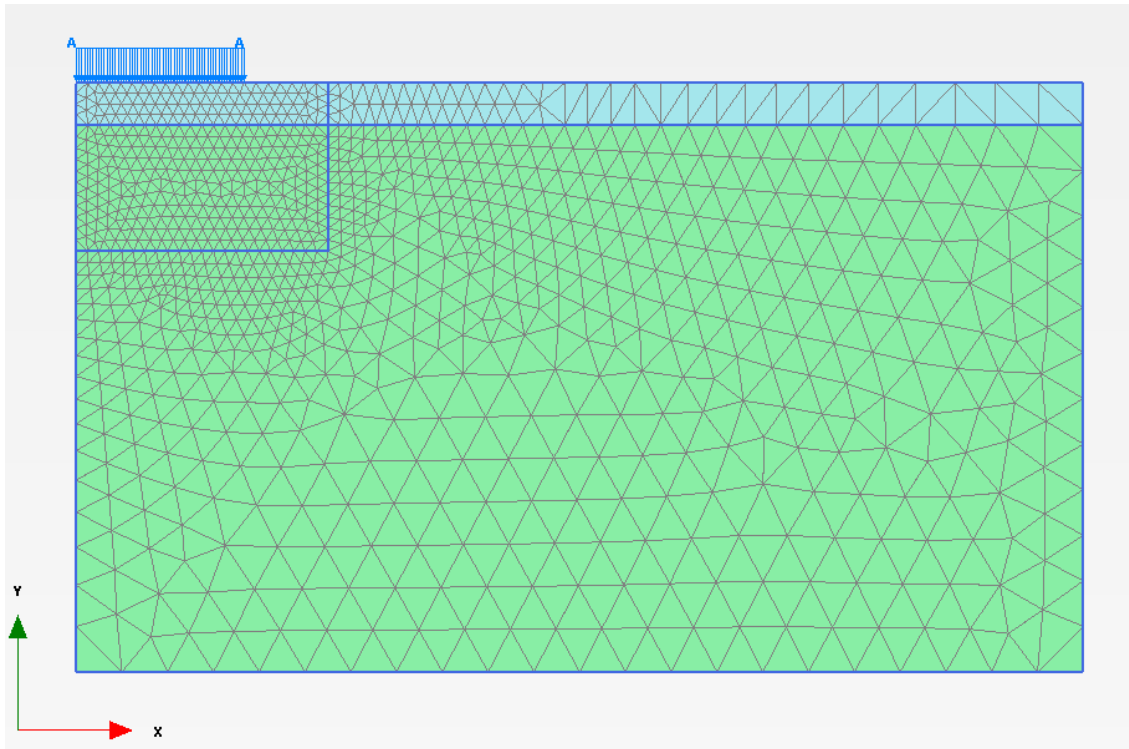
Jones (1962) presented a series of tables for determining the radial stress at the bottom of layer 1 (σ_{r1}), radial stress at the top of layer 2 (σ'_{r1}), radial stress at the bottom of layer 2 (σ_{r2}), radial stress at the top of layer 3 (σ'_{r2}), vertical stress at the interface of layers 1 and 2 (σ_{z1}), and vertical stress at the interface of layers 2 and 3 (σ_{z2}). The stresses in a three-layered system depends on the ratios k_1 , k_2 , A , and H , where k_1 is the ratio of elastic modulus of layer 1 to the elastic modulus of layer 2, k_2 is the ratio of elastic modulus of layer 2 to the elastic modulus of layer 3, A is the ratio of radius of the contact area to the thickness of layer 2, H is the ratio of thicknesses of layers 1 and 2. The parameters taken in the study are $k_1=20$, $k_2=2$, $H=1$, $A=0.8$. Table 1 shows the comparison of the stresses from PLAXIS and the solution proposed by Jones for the three-layered system. The results from PLAXIS are found to be in good agreement with the results from Jones, as shown in Table 3.1.

Table 3.1: Stresses in the three layered system

Stresses		Plaxis 2D	Jones table	Stress condition
Interface radial stress at the bottom of layer1	σ_{r1}	221.24	222.3	Tension
Interface radial stress at the Top of layer2	σ'_{r1}	2.79	2.77	compression
Interface radial stress at the bottom of layer2	σ_{r2}	3.84	4.00	Tension
Interface radial stress at the Top of layer3	σ'_{r2}	1.62	1.57	Compression
Vertical stress at the interface of layer1-2	σ_{z1}	14.64	14.61	Compression
Vertical stress at the interface of layer2-3	σ_{z2}	7.11	7.12	Compression

3.8 Abutment-soil System

Plane-strain finite element model with abutment wall and two-layered soil system was prepared as described in Section 3.2. Figure 3.9 shows the meshing of two-layered soil system with appropriate boundary conditions to indicate non-yielding abutment wall. The effect of various parameters, like moduli ratio and the thickness of the top layer on the stresses, are described next.

**Figure 3.9: Discretization of finite element model**

3.8.1 Effect of top layer thickness

3.8.1.1. Vertical Stress

It may be noticed that when the stiffer layer is present on the top of the softer layer, the stress dissipation occurs predominantly in the top layer. It can be inferred from the analysis that higher the thickness of the top stiffer layer, lower the vertical stresses developed in the top layer region (Figure 3.10).

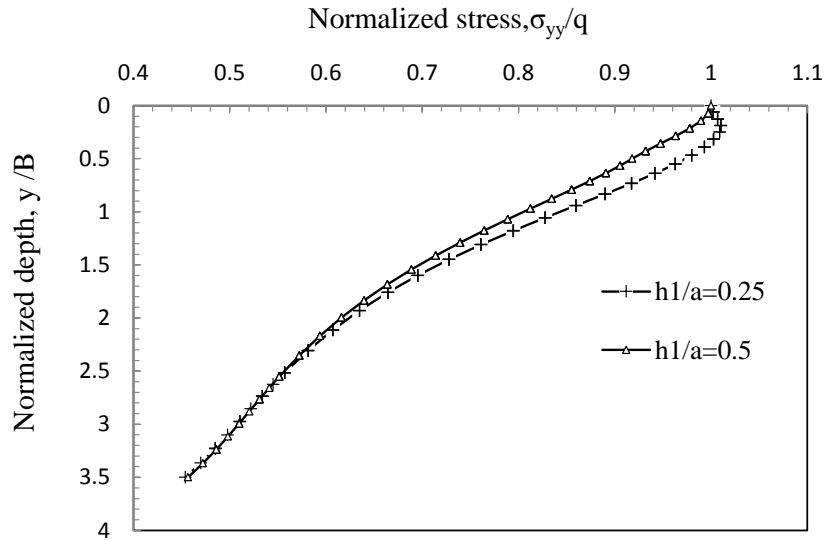


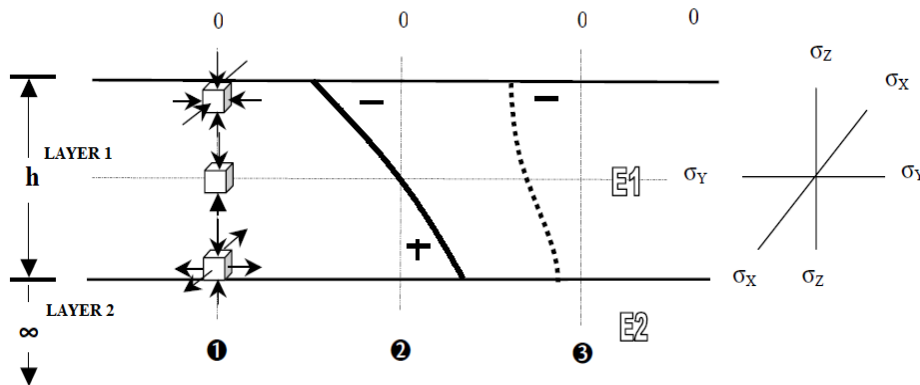
Figure 3.10: Effect of thickness of top layer on vertical stress

There is no significant reduction in the stresses in the bottom layer. Figure 3.10 shows the effect of thickness of the top layer on the distribution of vertical stresses under the center loaded area in a two layered system for moduli ratio equal to 5. There is no significant reduction of vertical stress at the interface of two layers for $h_1/a=0.25$. Vertical stress was reduced to about 8% for $h_1/a=0.5$. The effect of having higher thickness layer at the top produces a more significant change in the vertical stress.

Charts are proposed to predict the stresses within a two layered systems for different thicknesses of the top layer.

3.8.1.2. Lateral Stress

Figure 3.11 illustrates the behavior of lateral stress and vertical stresses in two-layered system. The modulus of the top layer is E_1 , modulus of the bottom layer is E_2 , and the thickness of top layer is represented as h . From Figure 3.11, lateral stress is found to change from compression to tension near the mid depth. The vertical stress is in compression but the magnitude has significantly decreased with depth.



Legend: - = (negative) compression, + = (positive) tension, ①-Principal stresses, ②-Horizontal stresses, ③-Vertical stresses

Figure 3.11: Three dimensional stress-state under the center of the load

Similar behavior is observed in the top layer where compressive stresses are produced at the top surface and tensile stresses are developed at the interface of top and bottom layers. The effect of top stiffer layer on the lateral stress is relatively small in the underlain layer.

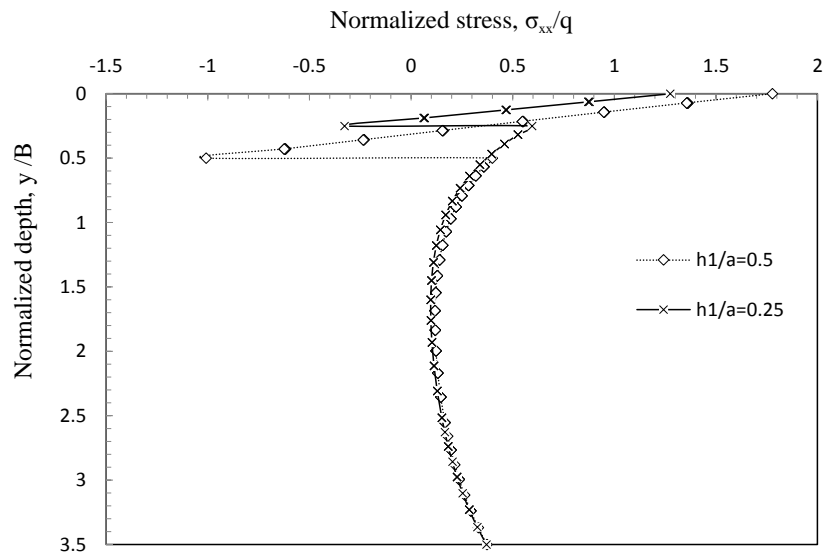


Figure 3.12: Effect of thickness in Lateral stress

It is observed from the Figure 3.12 that the Lateral stresses are 27% higher than the applied pressure as stresses at the top surface for the top layer thickness of 0.25. As the thickness of the top layer increases, there is an increase in the lateral stress significantly in the upper layer.

3.8.1.3. Settlement Profile

For a vertical pressure of 420.8kN/m², Figure 3.13 shows the settlement profile of the two layered abutment-soil system for different h_1/a ratios.

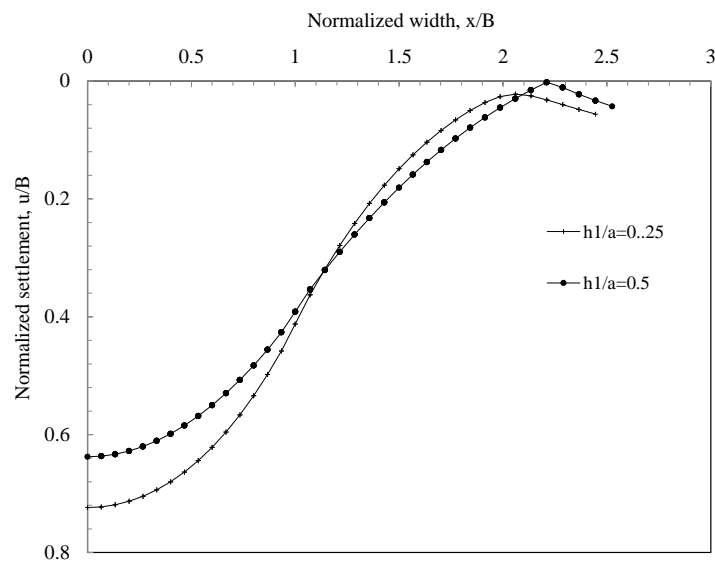


Figure 3.13: Effect of thickness in Settlement profile

Settlement of 0.64m below the center of the wheel load was obtained for $h_1/a=0.5$. Settlement decreases with an increase in the thickness of the top layer. For $h_1/a=0.5$, decrease in the settlement is about 10% from $h_1/a=0.25$ at the surface below the center of the load.

3.8.2 Effect of Moduli ratio

3.8.2.1. Vertical stress

Vertical stress distributions are shown for different moduli ratios (E_1/E_2) for $h_1/a=0.5$ (Figure 3.14). Increase in the moduli ratio reduces the stress in the soil. At the interface, the vertical stress is about 86% of the applied pressure. Reduction in the vertical stress is more significant for $E_1/E_2=10$.

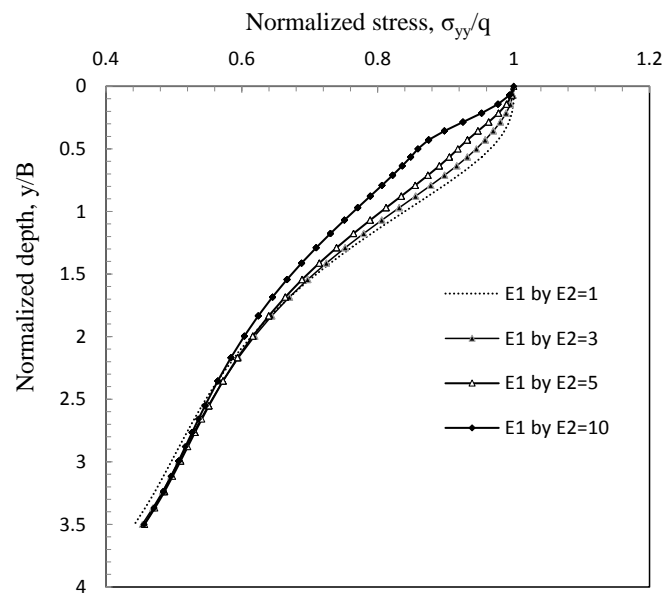


Figure 3.14: Effect of moduli ratio in Vertical stress

It is also found from the literature by Nagengra prasad [13] that the moduli ratio equal to 10 seems to have optimum effect on stress dissipation. This turns out that if the top layer has stiffness 10 times greater than the underlying layer, the applied pressures would be dissipated in the upper layer reducing the stress in the lower layers and thus reducing the settlements.

3.8.2.2. Lateral stress

Figure 3.15 shows the lateral stress distribution on two-layered soil system for different moduli ratio for $h_1/a=0.5$. It is inferred from the plot that higher the moduli ratio, the higher the stress value in the top stiffer layer.

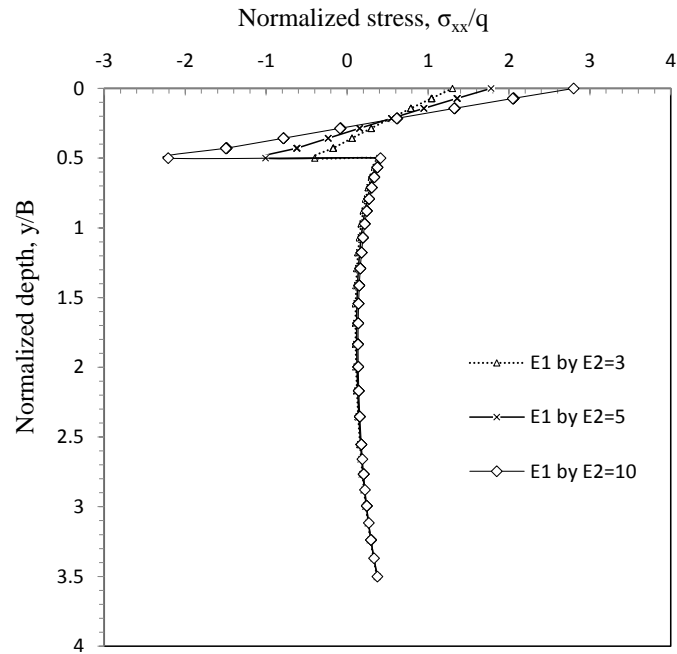


Figure 3.15: Effect of moduli ratio in Lateral stress

There is no significant increase in the bottom layer. Compressive stresses are developed at the surface and it changes from compression to tension somewhere in the mid depth. Stress increase in the compressive region at top is about 30% for $E_1/E_2=3$.

3.8.2.3. Settlement Profile

Figure 3.16 shows the settlement profile at the surface for different moduli ratio for 1m width of load for the case of $h_1/a=0.5$. The profile shows that the increase in the stiffness of the top layer reduces the settlement at the surface. For $E_1/E_2=5$ decrement in the settlement is about 4% when compared with the case with moduli ratio $E_1/E_2=3$. As mentioned in the previous section, $E_1/E_2=10$ ratio gives a significant level of improvement and the settlement reduced by 12% when compared to $E_1/E_2=3$.

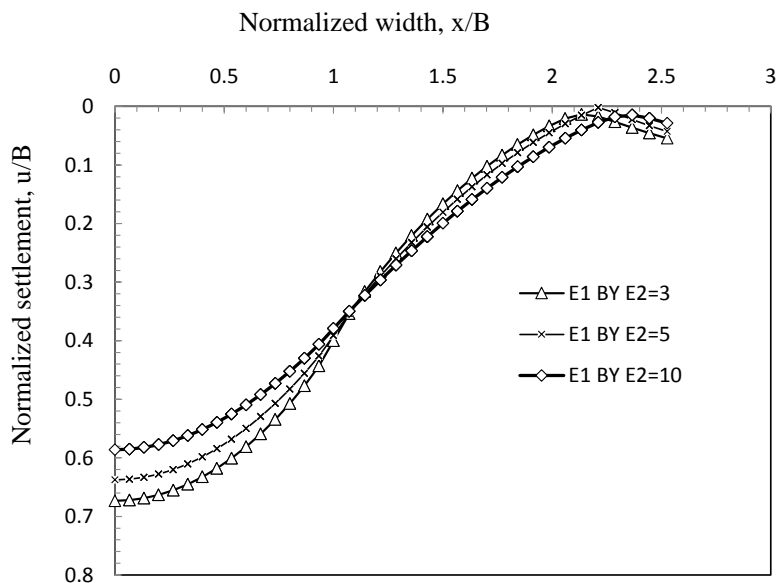


Figure 3.16: Effect of moduli ratio in settlement profile

Chapter 4

Modeling Abutment-Soil System in PLAXIS 3D

4.1 Introduction

Representation of axle wheel load acting on Abutment-soil system as a distributed strip load does not realistically represent the actual distribution of the stresses on the wall, due to 3D nature of the problem. Hence, modeling the problem in 3D finite elements will be more appropriate. Axle wheel loading for the carriage way behind the abutments in contact with the earth are covered in IRC 6-2000. Wheel load on the backfill not only produces non-uniform stress throughout the wall height but also a bell-shaped variation along the width of the wall. To account for this stress variation along both the width and depth of the wall, an approach of redistributing the lateral stresses over a certain width is followed. A brief description about the approach is explained in Section 4.6. In this Chapter, details on 3D finite element model – element types, meshing, and loading conditions– are explained. Model consists of two-layered system with base course layer overlying the embankment fill material. Effects of location of load (measured from the wall face) and the moduli ratio (of the layers of two-layered or three-layered systems) on the lateral stress distribution were studied for various lane widths. Figures 4.1 and 4.2 show the photograph and schematic of approach slabs provided for a smooth transition between the bridge deck and the roadway pavement.



Figure 4.1: Bridge abutment of a Highway bridge

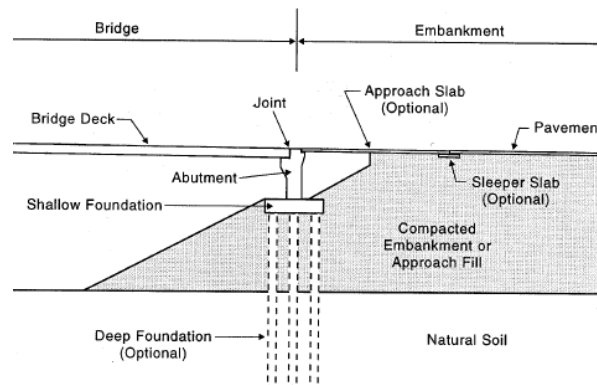


Figure 4.2: Bridge abutment backfilled with embankment fill

In the present study, abutment-soil system was modeled considering two cases- (a) two-layered system with a granular base layer/approach slab resting on the embankment fill material, and (c) three-layered system with an approach slab over the granular base layer resting on the embankment fill material.

4.2 Problem Definition and Objectives of the Study

In bridge construction, the bridge abutments are backfilled with embankment material and an approach road laid over the fill. Approach slab is provided between the bridge structure and the approach road (as shown in Figure 4.3) to give a smooth transition between the bridge structure and the approach road. Elastic solutions are available in the literature to calculate the lateral stresses due to homogeneous backfill for standard loading conditions, for example, point load, strip load, line load, etc. These solutions are not applicable for the problem of bridge abutment with a layered system and for wheel loads acting on finite contact areas. The objective of the study is to find the lateral stress distribution on the abutment due to the wheel loads. In this study, lateral stresses on the abutment as per the Indian Road Congress (IRC) standard design loadings (specified in IRC-6-2000, Section II) are calculated. This loading consists of a wheel load train with a driving vehicle and two trailers of specified axle spacings.

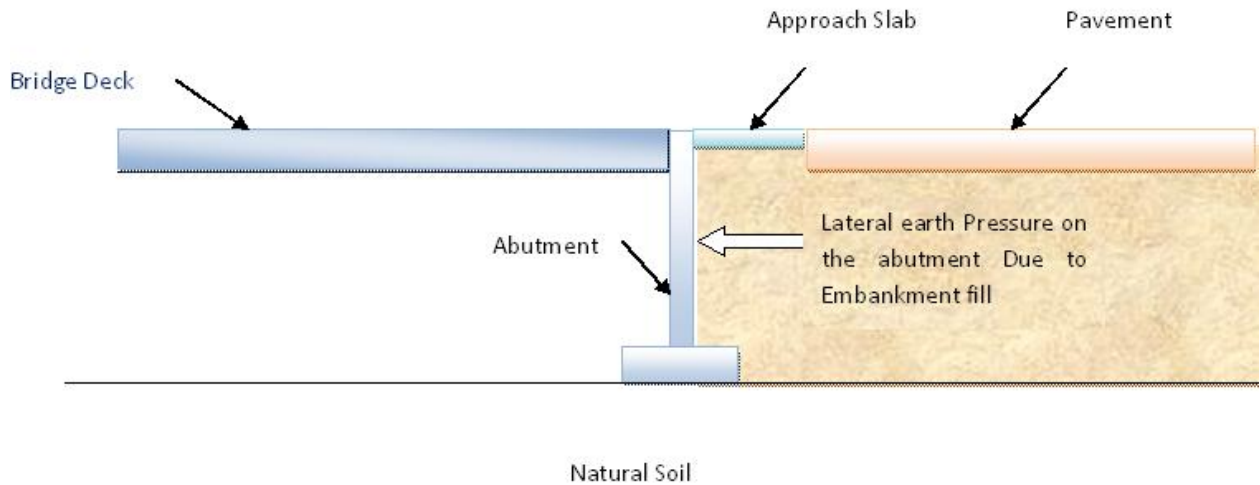


Figure 4.3: Definition sketch of the problem

4.3 Finite element Model

A Three dimensional (3D) finite element analysis was performed using PLAXIS 3D. Figure 4.4 shows the isometric view of the model of abutment-soil system for a two lane highway of 5.3m width and 6m wall height. The model is shown for the case with the granular layer overlying the embankment fill material. Thickness of the granular base layer resting on the embankment backfill is 300mm. The lateral boundary is extended to a distance of 3.7 times the lane width. This boundary distance is found to eliminate boundary effects on calculated stresses or displacements. Sections 4.4 and 4.5 provide details on the meshing quality and the boundary conditions adopted.

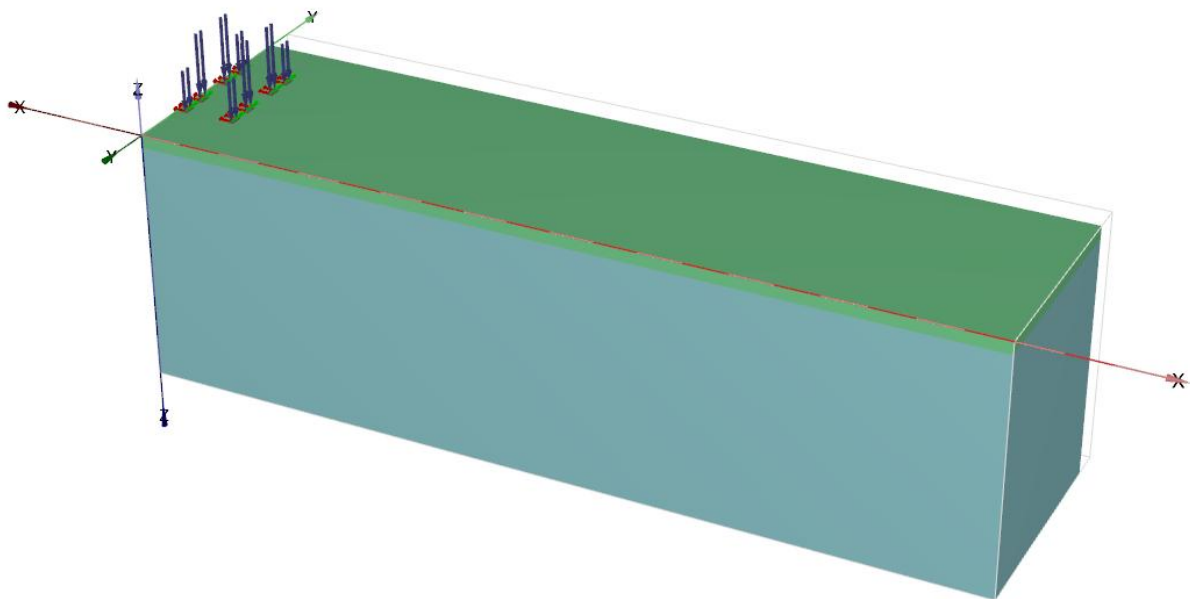


Figure 4.4: Isometric view of Abutment-soil system in PLAXIS 3D

4.3.1 Finite elements

10-noded-tetrahedral elements are used to model the soil layers and other volume clusters. Similar to 2D finite element model, 15-noded-triangular and 6-noded-triangular elements are used to model the area elements. This type of element involves second-order interpolation for displacements and numerical integration involves four Gauss points (also called as stress points). Figure 4.5 shows the position of nodes and the stress points in 10-noded-tetrahedral soil element.

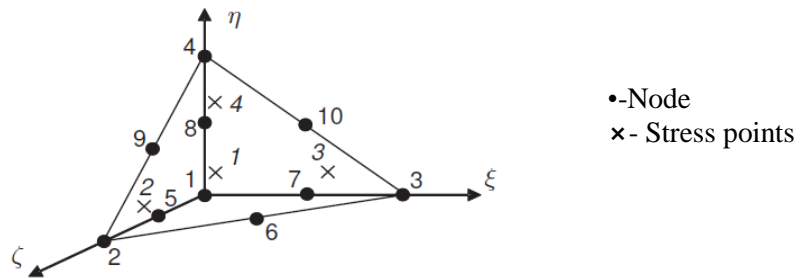


Figure 4.5: Position of Nodes and Stress points in the element

4.3.2 Plate elements

Plate elements are different from the 6-noded triangles in the sense that they have six degrees of freedom per node instead of three, i.e., three translational degrees of freedom (d.o.f.s) (u_x, u_y, u_z) and three rotational d.o.f.s (ϕ_x, ϕ_y, ϕ_z) . These elements are directly integrated over their cross section and numerically integrated using three-point Gaussian integration. Figure 4.6 shows the position of the integration points.

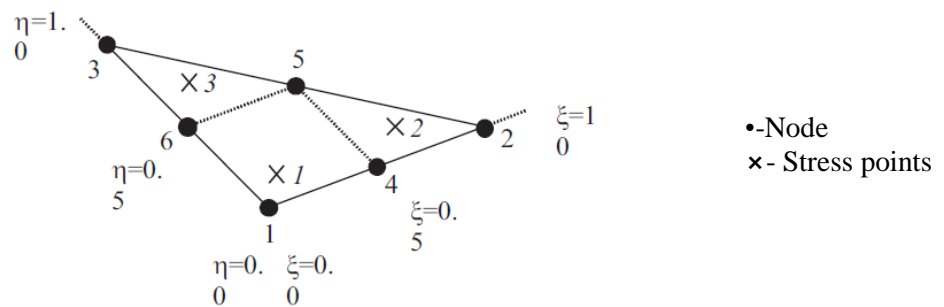


Figure 4.6: Local numbering and position of nodes and integration points of a 6-noded-triangle

4.3.3 Interface elements

The importance of using interface elements is explained in Section of 3.4 (Chapter 3). In PLAXIS 3D, when using 15-noded soil area elements, the corresponding interface elements are defined by eight pairs of nodes and eight stress points. Corners in stiff structures and an abrupt change in boundary may lead to peaks in stresses and strains. Volume elements are not capable of reproducing these sharp

peaks and will, as a result, produce non-physical stress oscillations. The problem can be solved by the use of interface elements as shown in Figure. 4.7

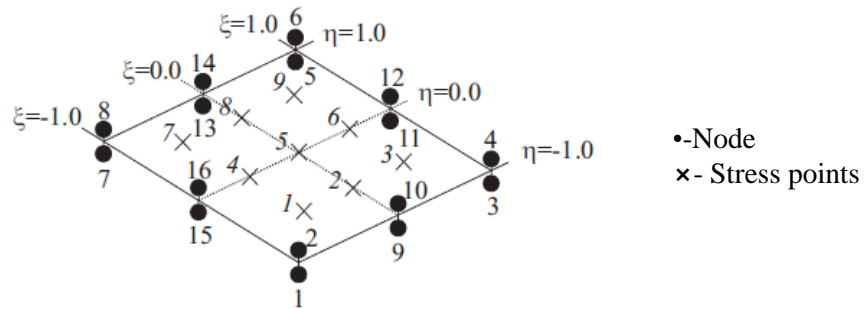


Figure 4.7: Local numbering and position of nodes and integration points of an interface element

Interface elements are extended below or around the corner of the structures used in the analysis in order to avoid stress oscillations. These are not meant to model soil-structure interaction, but to allow for sufficient flexibility. The strength reduction in the interfaces should not be considered in such cases.

4.3.4 Meshing

Details on different types of global and local coarseness of meshing available in PLAXIS along with the meshing procedure are briefly explained in Section 3.6 (Chapter 3), which holds good for three-dimensional model as well. Perfect face of a mesh element consists of an equilateral triangle to improve the mesh quality and sharp angle should be avoided as shown in Figures 4.8 (a) and (b). In areas, where large stress concentrations or large deformation gradients are expected, it is desirable to have a fine or very fine finite element mesh, whereas other parts of the geometry might not require a fine mesh.



Figure 4.8: Improved mesh quality

Such a situation often occurs when the geometry model includes edges or corners or structural objects. This can be handled by using local coarseness parameter in addition to the global coarseness parameter. These parameters give an indication of the relative element size with respect to the average element size as determined by the global coarseness parameter.

4.4 Validation studies

Validation of the model was carried out with the available solution. A Plane-strain model was considered to compare the vertical stresses obtained from PLAXIS 2D and 3D models. Load of magnitude equal to 94.4kN/m^2 (total load from two front wheels applied over wheel-ground contact area equal to $0.15\text{m} \times 3.8\text{m}$; 0.15m represents the width of wheel-ground contact in X direction and 3.8m represents one-lane carriageway width in Y direction for the 3D model) was applied as a strip load acting at the edge of the abutment. The results from PLAXIS 3D are compared with the results of PLAXIS 2D. Figure 4.9 shows the comparison of the results and it is evident that the model developed in PLAXIS 3D shows a good agreement with the results from PLAXIS 2D. This validated that the meshing and boundary conditions are appropriate in the model developed in PLAXIS 3D for a simple case of a plain strain problem.

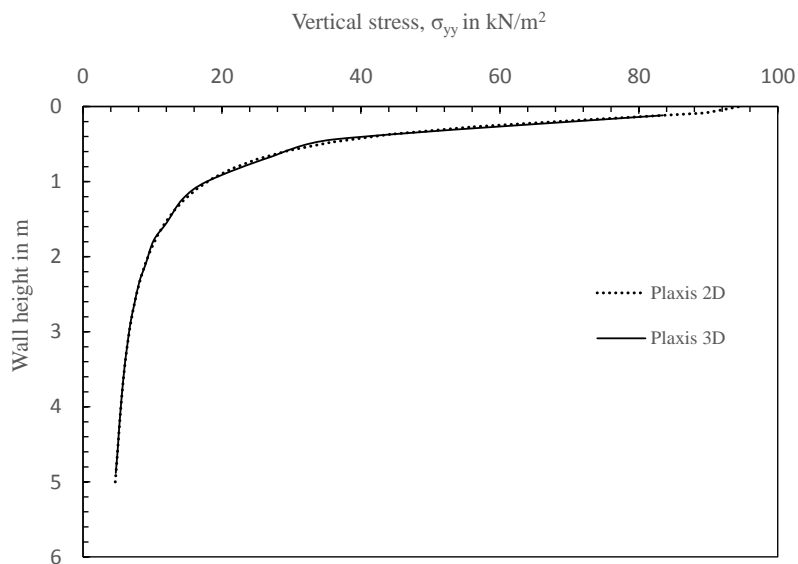


Figure 4.9: Comparison of vertical stresses from PLAXIS 3D with PLAXIS 2D results for a plane-strain loading

4.5 Methodology

Figure 4.10 (a) shows non-uniform lateral stress distribution on the wall and the maximum stress developed along the depth and width directions. Figure 4.10(b) shows a bell-shaped lateral stress distribution along the width of the carriage way and is symmetric about the centroid of the load applied along the width of the carriage way.

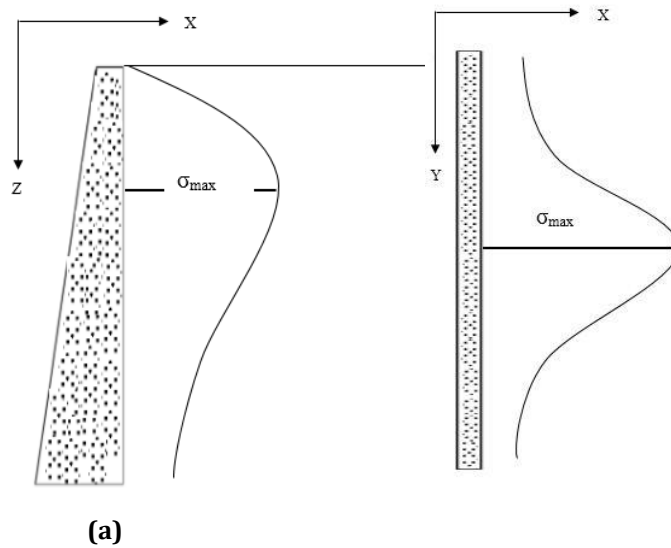


Figure 4.10: Lateral stress distribution along (a) wall height, and (b) width of the carriage way

4.6 Equivalent live load surcharge

A method is proposed to replace the axle wheel load surcharge with that of a uniform surcharge applied at the ground surface. This equivalent uniform surcharge can be used to calculate the lateral stresses that account for the bell-shaped stress variation. At a given depth, the stress variation due to front axle wheel loads is as shown in Figure 4.11. In order to calculate the equivalent forces at any depth, an increment, β , equal to 0.4m, was considered along the width of the wall and the lateral stresses are integrated numerically along the width using trapezoidal procedure. When the average lateral stress at any depth is determined, the equivalent live load surcharge is obtained using equivalent force and bending moment methods. These methods are explained next.

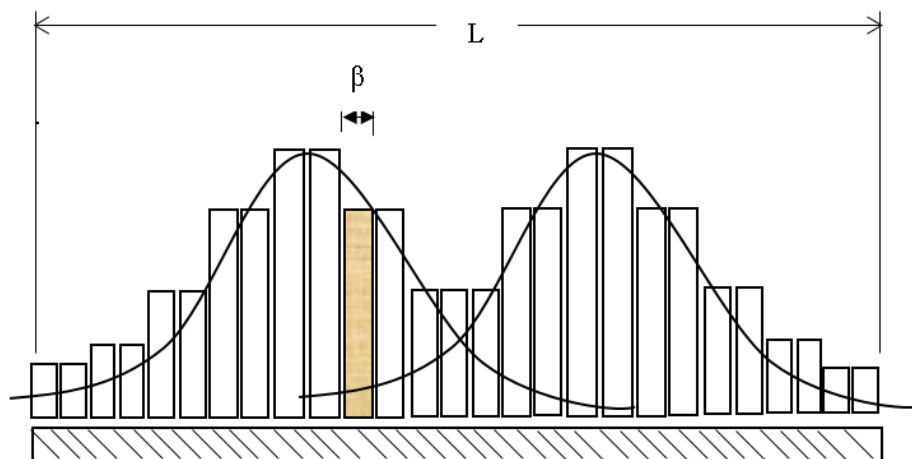


Figure 4.11: Approximate method of calculation of average lateral stress at any depth of the wall

4.6.1 Equivalent Bending moment and Force methods

In order to convert the actual lateral stress into equivalent uniform surcharge, the equivalent bending moment and the equivalent force methods are followed. In the bending moment method, the moment

obtained from the numerical integration of moments (Fig. 4.12(b)) is equated with the moment that would be obtained when replaced with a uniform surcharge at the ground surface (Fig. 4.12(a)).

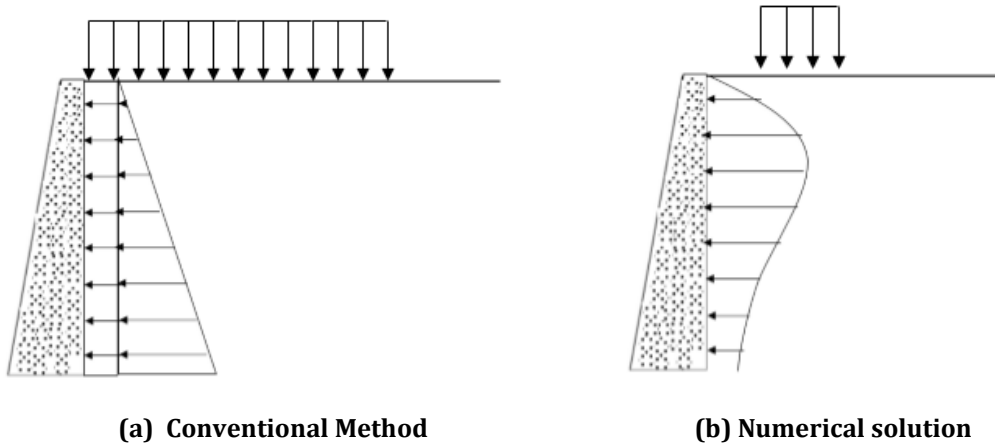


Figure 4.12: Forces acting on the wall due to (a) Uniform surcharge, and (b) live load due to wheel loads.

When replaced with uniform surcharge at the ground surface, the live load from vehicles are considered as an additional height of earth that produces a uniform stress as shown in Figure 4.12 (a). The moment produced by the uniform stress at $z = H$ is given in Equation [4.1].

$$M_c = \frac{1}{2} K \gamma h_{eq} H^2 \quad (4.1)$$

where,

K = Co-efficient of lateral earth pressure

γ = Unit Weight of the embankment backfill

H = Wall height

The vehicular loading given in IRC 6-2000 (explained in Section 4.1) does not produce uniform lateral stress against the wall. A Constant stress may be assumed over each increment (β) of wall height, the bending moment at depth z about the wall base is given by Equation [4.2],

$$M_E = z \sum_{i=1}^n \beta \sigma_i - \sum_{i=1}^n d_i \beta \sigma_i \quad (4.2)$$

where,

z = Wall height in m

β = Increment of wall height

σ_i = Lateral stress at depth d_i

d_i = Distance from the surface to the point where σ_i is applied

i = Integer ranging from 1 to the number of increments, n

Equating the moments about the base of the wall due to uniform equivalent surcharge (Eq. (4.1)) with the moments calculated from numerical solution due to actual stress distribution due to wheel loads (Eq. (4.2)) gives the equivalent height of surcharge. The equivalent height of surcharge is given by Equation [4.3]

$$h_{eq} = \frac{2M\bar{\xi}}{k\gamma H^2} \quad (4.3)$$

4.7 Loading condition as per IRC 6-2000

4.7.1 Class AA Loading

Figure 4.13 illustrates the vehicle contact area, spacing between wheels and the wheel configuration that are used in the study as per Class AA loading outlined in IRC 6-2000.

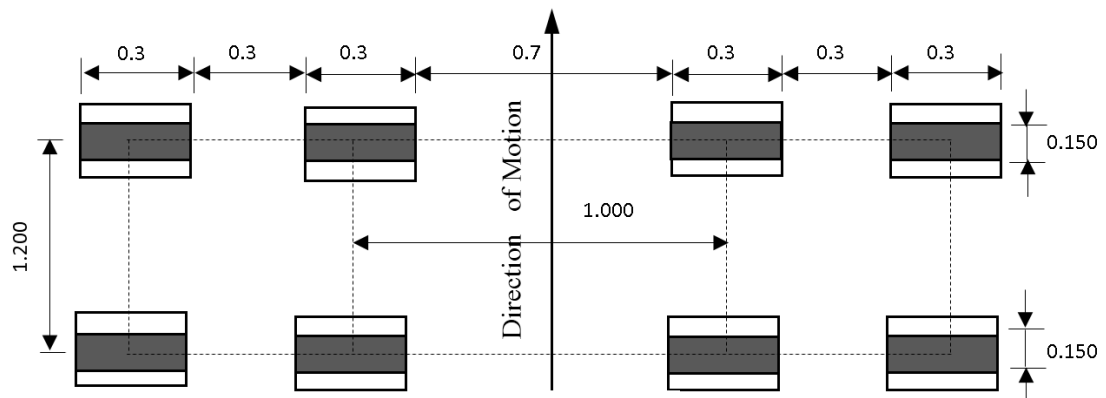


Figure 4.13: Plan view of IRC Class AA Loading (all dimensions are in m).

Figure 4.14 shows the elevation view of the Class AA loading with the axle load from each wheel and the spacing between the wheels.

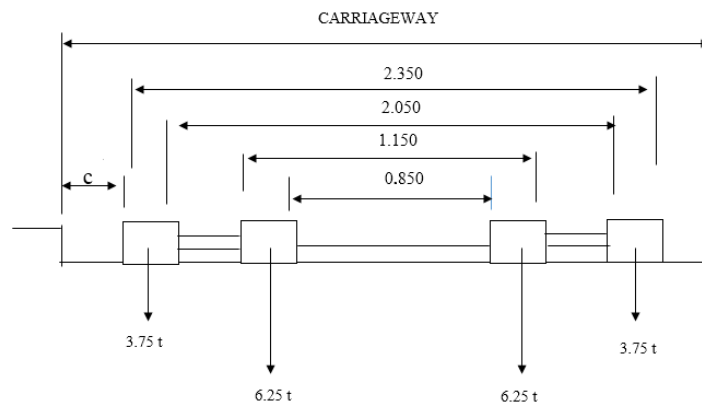


Figure 4.14: Elevation view of IRC Class AA Loading (all dimensions are in m).

4.7.2 Class A Loading

Figure 4.15 illustrates the spacing between wheels as per Class A loading specified in IRC 6-2000. It consists of a train of axle vehicle where the contact area and the load vary. Table 4.1 provides the ground contact area for various axle loadings. The dimensions of the contact area are represented by B and W. Figure 4.16 provides the elevation view of the axle wheel loads corresponding to Class A loading. All the loads indicated in the Figure are given in tons.

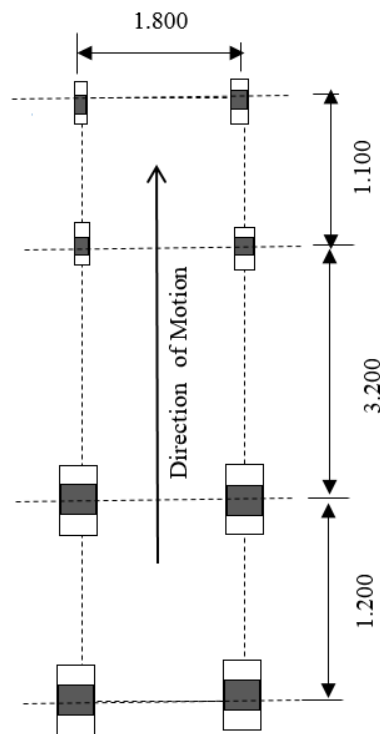


Figure 4.15: Plan view of IRC Class A Loading (all dimensions are in m).

Table 4.1: Ground contact area of wheels for Class A Loading

Axle load in tons	Ground contact area	
	B(mm)	W(mm)
11.4	250	500
6.8	200	380
2.7	150	200

Table 4.2: Minimum clearance between the road face of the kerb and the outer edge of the wheel

Carriageway width	Minimum value of C (m)
Single-Lane Bridges	
3.8m and above	0.3
Multi-Lane Bridges	
Less than 5.5m	0.6
5.5m or above	1.2

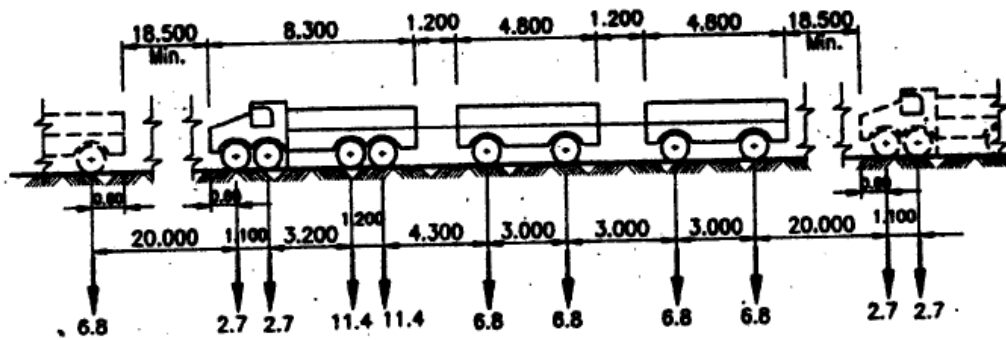


Figure 4.16: Elevated view of Multi-axle IRC Class A Loading

Table 4.3: Live load combination as per IRC 6-2000

Carriageway width	Number of lanes	Load combination
Less than 5.3m	1	One lane of class A considered to occupy 2.3m. The remaining width of carriageway shall be loaded with 500kg/m ²
5.3m and above but less than 9.6m	2	One lane of class 70R or two lanes of class A
9.6m and above but less than 13.1m	3	One lane of class 70R with one lane of class A or three lanes of class A
13.1m and above but less than 16.6m	4	One lane of class 70R for every two lanes with one lane of class A for the remaining lanes, if any, or one lane of class A for each lane
16.6m and above but less than 20.1m	5	One lane of class 70R for every two lanes with one lane of class A for the remaining lanes, if any, or one lane of class A for each lane

Table 4.3 provides the live load combination (IRC 6-2000) used in the present study. The load combination is provided for various carriageway widths and number of lanes. Minimum distance should left from the kerb to the edge of the wheel should be as per Table 4.2 for different lane widths.

4.8 Lateral stress distribution considering Two-layered system

4.8.1 Two Lanes

Firstly, the lateral stress distribution is obtained for two-lane roadway considering two types of loadings commonly adopted for permanent bridges – Class AA loading and Class A loading. The unit weight of the soil, γ , was taken as 18kN/m^3 . The earth pressure coefficient, K , was taken to be a function of Poisson's ratio, ν , expressed as $K=\nu/(1-\nu)$. $\nu=0.3$ was considered for both the layers. Two-lane widths equal to 5.3m to 7.0m are considered. The loading conditions for different lane widths are explained in IRC 6-2000 (Table.4.1). Stresses are obtained for various distances, D , of the front wheel load measured from the wall face.

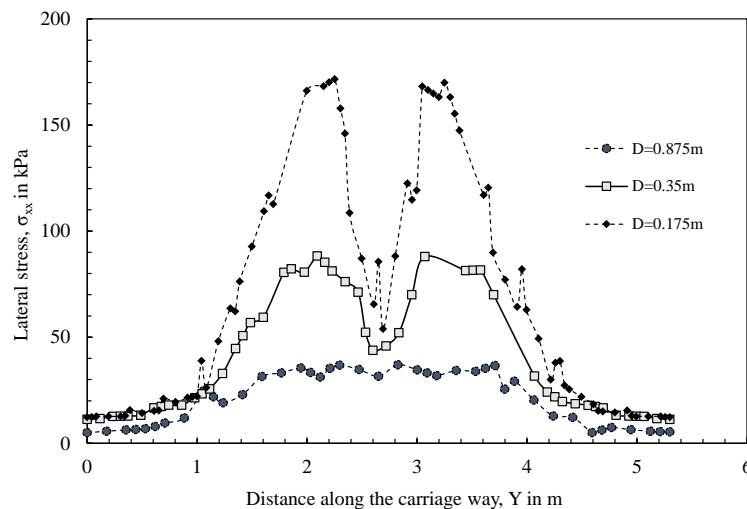


Figure 4.17: Lateral stress distribution along 5.3m lane width at a depth of 0.2m for $E_1/E_2=4$ for various distances of D equal to 0.175m, 0.35m and 0.875m

The loading configuration such as spacing between the wheels, ground contact area (B and W) of each wheel, axle load coming from each wheel, and minimum clearance to be considered from the kerb are briefly given in Section 4.7. Load combinations corresponding to a specific lane width (given in Table 4.2) are used in the study.

Figure 4.17 shows the variation of lateral stress along the 5.3m lane width for different D values at a depth of 0.2m due to Class AA loading. It can be seen that the maximum lateral stress is developed at the center of the wheel load and this maximum lateral stress becomes less pronounced for large values of D . The lateral stress distribution (shown at a depth of 0.2m) decreases as the front wheel moves away from the wall face. The position of wheels that produces the maximum stresses is considered as the critical value for design. The percentage increase in the maximum lateral stress is about 50% when the front wheels are placed at 0.175m compared to that when the front wheels are located at 0.35m from the wall face.

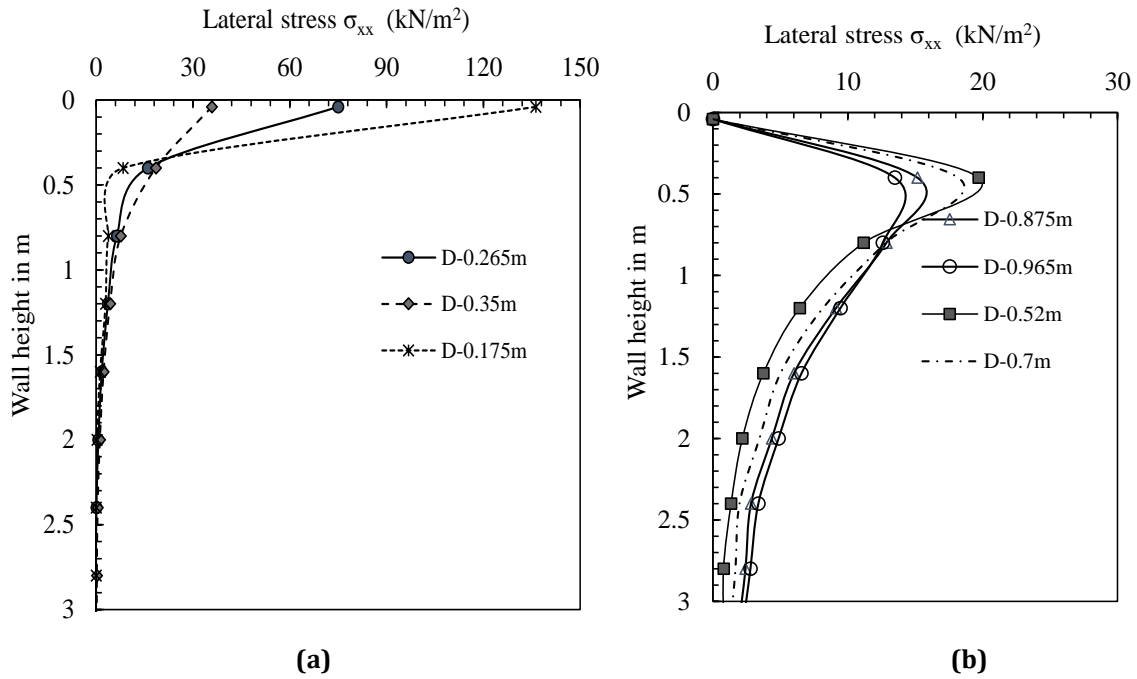


Figure 4.18: Average lateral stress distribution of 5.3m lane width for various distances of D for $E_1/E_2=4$ for (a) $D = 0.175$ to 0.35 m, and (b) $D=0.525$ to 0.965 m

Average lateral stress at every 0.4m increment along the depth of the wall was determined by numerically integrating the area under the curve along the width using trapezoidal procedure. Figure 4.18 shows the variation of average lateral stress for different values of D for $E_1/E_2=4$. As the front wheel of the vehicle moves away from the face of the wall, the lateral stress intensity decreases. It can also be observed that $D=0.175$ m produces lateral stresses higher than that for other D values. Hence, the critical lateral stresses are generated on the wall when the wheel load is located at a distance of 0.175m from the face of the wall. For further analysis on the variation of lateral stresses on the wall, $D=0.175$ m is only considered.

4.8.1.1. Variation of lateral stress with depth for $E_1/E_2=4.0$ and 8.0

It can be observed from Figure 4.19 that significant lateral stresses develop in the top layer. For the case of $E_1/E_2=4$, lateral stress equal to 192kPa develops at the surface, while this value increases by about 42% for the case of $E_1/E_2=8$. The lateral stresses developed in the bottom layer are found to be almost negligible.

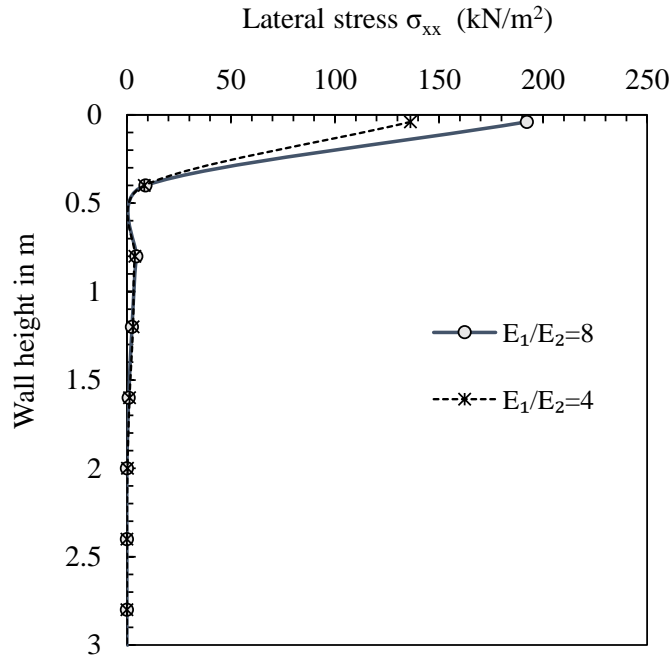
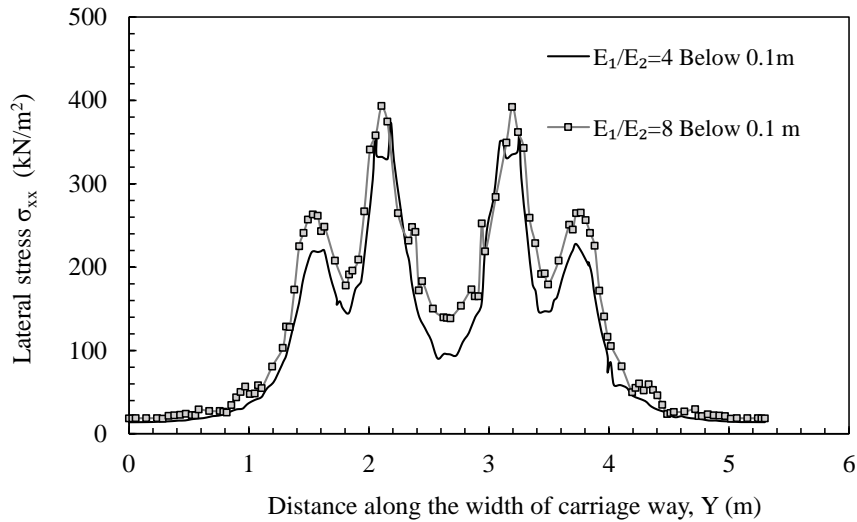


Figure 4.19: Average lateral stress distribution for $E_1/E_2=4.0$ and 8.0 when $D=0.175\text{m}$.

4.8.1.2. Variation of lateral stress with carriageway width for $E_1/E_2=4.0$ and 8.0

Figure 4.20(a) shows the variation of lateral stress at a depth of 0.1m for $E_1/E_2=4.0$ and 8.0 . The top layer thickness is 0.3m and the lateral stress within the top stiff layer produces higher stresses when $E_1/E_2=8.0$ which is due to the fact that most of the stresses will be dissipated in the stiff layer. Peak values of lateral stresses are found at exactly below the center of each load.



(a)

Figure 4.20: Lateral stress distribution along 5.3m lane width at a depth of 0.1m for $E_1/E_2=4.0$ and 8.0

The maximum stress occurs at the center of the wheels, since the load is of larger magnitude. Maximum lateral stress produced by $E_1/E_2=8$ is about 15% more compared to that of $E_1/E_2=4$ at a depth of 0.1m below the surface of the top layer.

Figure 4.20(b) shows the lateral stress distribution along the lane width of 5.3m for $E_1/E_2=4$ and 8 at different depths (0.8m-to2.8m). In the case of $E_1/E_2=4$, at any depth in the bottom layer the lateral stress developed is larger than that compared to $E_1/E_2=8$. This can be explained by the theory of two-layered system where higher the moduli ratio, the larger the stresses developed in the top layer leading to lower stresses being transferred to the bottom layers.

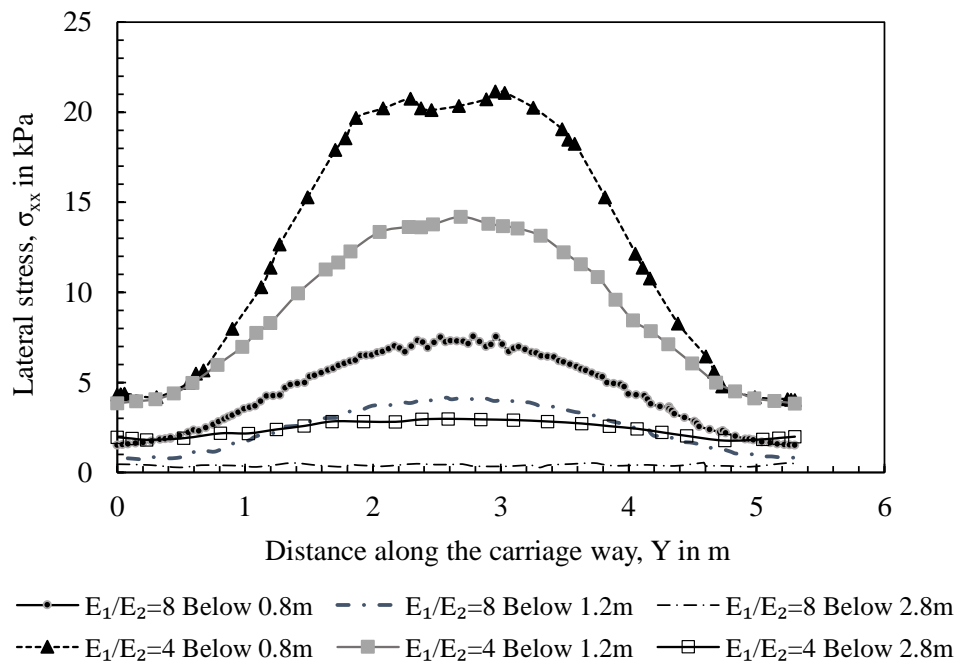


Figure 4.20: Lateral stress distribution of 5.3m lane width at different depths of $z=0.8\text{m}$, 1.2m and 2.8m for $E_1/E_2=4.0$ and 8.0

4.8.1.3. Variation of lateral stress with depth for $E_1/E_2=4.0$

As explained in Section 4.2.3, most of the stresses get dissipated in the top stiffer layer. Figure 4.21 shows the lateral stress along the lane width at various depths in the bottom layer for $E_1/E_2=4$. The lateral stresses show a bell-shaped variation and the bell-shaped nature reduces with the increase in depth. Beyond a depth of 2.8m, the lateral stresses variation along the lane width remains a constant value.

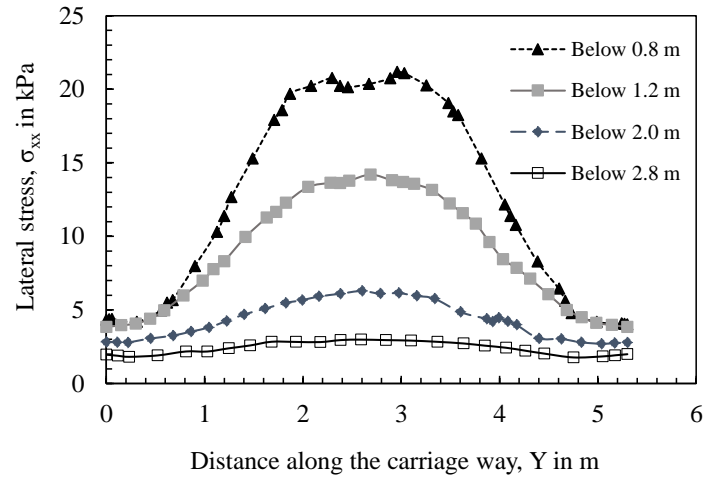


Figure 4.21: Lateral stress distribution of 5.3m lane width for $E_1/E_2=4$ for different depths of $z = 0.8\text{m}, 1.2\text{m}, 2.0\text{m}, 2.8\text{m}$

4.8.2 One Lane

For the case of lane width less than 3.8m, the roadway is designed as single-lane highway. In this study, lane width of 3.8m is considered. IRC Class A Loading is considered in the analysis and the loading configuration is as explained in Section 4.7. Two-layered system with the granular base layer over the embankment fill was modeled. Poisson ratio, $\nu = 0.3$, is considered in both the layers. The effects of moduli ratio on the lateral stress along depth and width directions are studied.

4.8.2.1. Variation of lateral stress with depth for $E_1/E_2=4.0$ and 8.0

Increase in the moduli ratio (E_1/E_2) produces an increase in the lateral stress at the top layer. It infers that most of the stresses get dissipated within the top layer for higher E_1/E_2 . For instance, Figure 4.22 shows the variation of average lateral stress with depth for $D=0.175\text{m}$ and for two values of moduli ratios ($E_1/E_2=4.0$ and 8.0). At the surface, the lateral stresses for $E_1/E_2=8.0$ is about 30% higher than that for $E_1/E_2=4.0$.

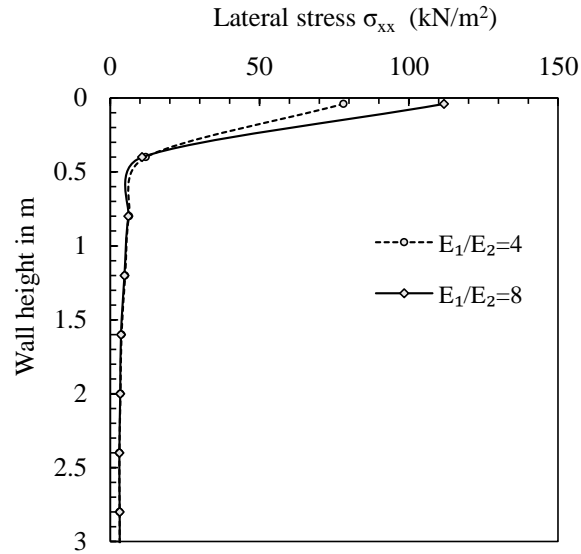


Figure 4.22: Average lateral stress distribution for $D=0.175\text{m}$ for $E_1/E_2= 4.0$ and 8.0

4.8.2.2. Variation of lateral stress with carriageway width for $E_1/E_2=4.0$ and 8.0

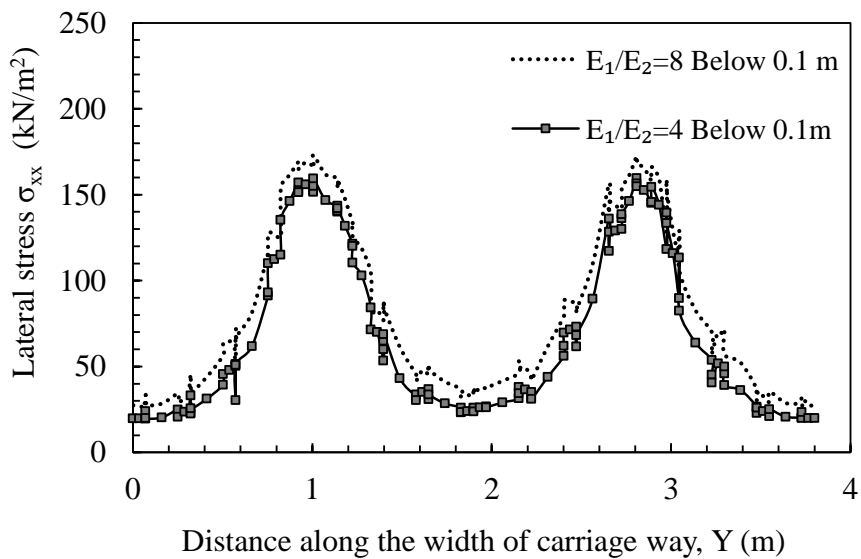


Figure 4.23: Lateral stress distribution of 3.8m lane width for $E_1/E_2=4$ and 8 at different depth of $z = 0.1\text{m}$

Figure 4.23 shows the effect of the moduli ratio ($E_1/E_2=8.0$ and 4.0) within the top layer at a depth of 0.1m . At shallow depths from the top surface (say 0.1m), two peak lateral stresses are observed. It is observed that the maximum lateral stress developed was 10% higher for $E_1/E_2=8$ than that compared to $E_1/E_2=4$.

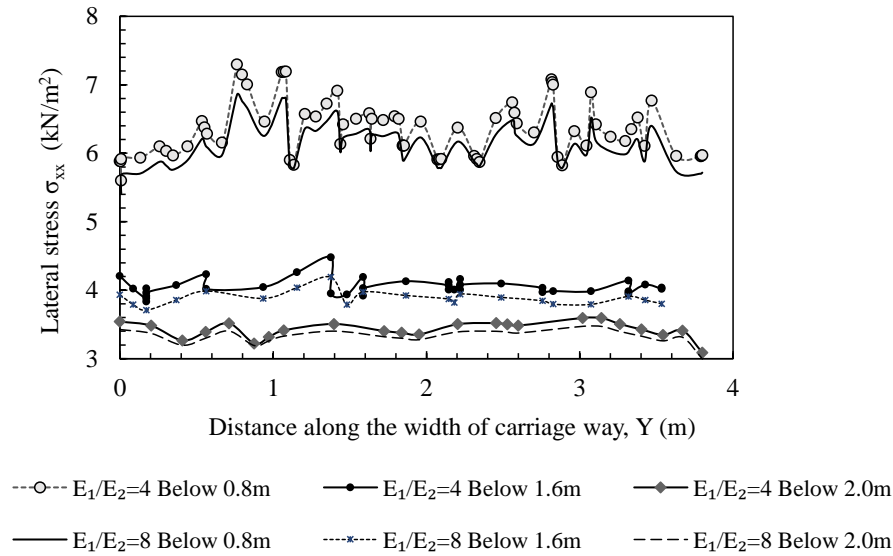


Figure 4.24: Lateral stress distribution of 3.8m lane width for $E_1/E_2=4$ and 8 at different depths of $z = 0.8\text{m}$, 1.6m and 2.0m

Figure 4.24 shows the variation of lateral stress distribution along 3.8m lane width for $E_1/E_2=4.0$ at different depths of $z=0.8\text{m}$, 1.6m , 2.0m . For larger E_1/E_2 values, lateral stresses are dissipated in the top stiff layer and hence for depths below the top layer, the lateral stresses for larger $E_1/E_2 (=8.0)$ are found to be lower than that for lesser $E_1/E_2 (=4.0)$.

4.8.3 Three Lanes

Lane width for three lane highway was taken as 9.6 m. As given in Table 4.1, the loading condition is Class AA load for every two lanes. The effects of E_1/E_2 on lateral stresses developed in the top and bottom layers for three lane highway are presented next.

4.8.3.1. Variation of lateral stress with depth for $E_1/E_2=4.0$ and 8.0

Figure 4.25 shows that the average lateral stresses at the surface of backfill for $E_1/E_2= 8$ are 40% higher than that for $E_1/E_2=4$. For depths beyond 0.4m , the lateral stresses on the abutment are found to be negligible.

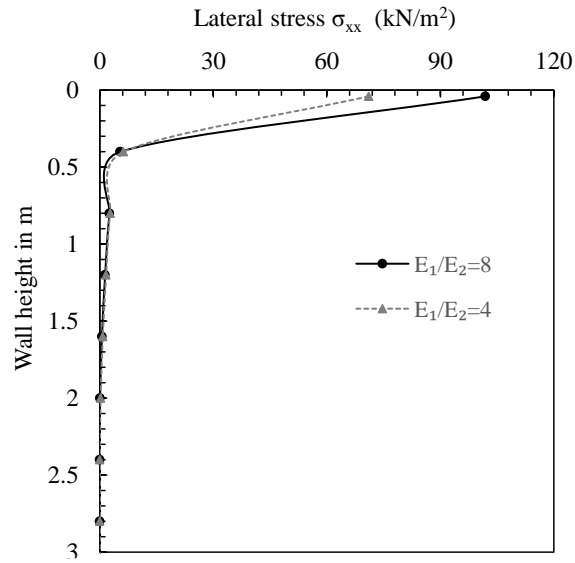
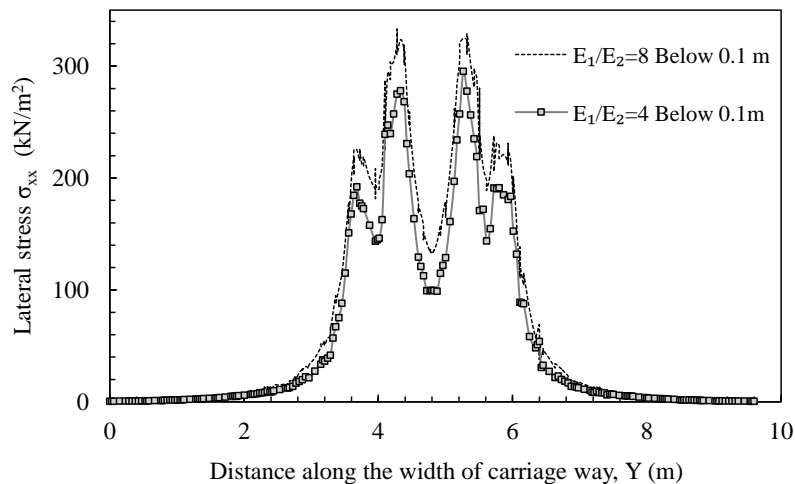


Figure 4.25: Average lateral stress distribution for $D=0.175\text{m}$ for $E_1/E_2=4.0$ and 8.0

Figure 4.26(a) shows the variation of lateral stress with the width of carriageway within the top stiff layer at a depth of 0.1m for $E_1/E_2=4.0$ and 8.0 . Figure 4.26 (b) shows the variation of lateral stress with the width of carriageway within the bottom layer at different depths of 1.2m, 1.6m, 2.0m for $E_1/E_2=4.0$ and 8.0 .

4.8.3.2. Variation of lateral stress with carriageway width for $E_1/E_2=4.0$ and 8.0

It is also observed from Figure 4.26(a), that the effect of E_1/E_2 within the top layer is more significant in three lanes than in two lanes. For instance, for lane width of 9.6m the increase in the lateral stress is 17 % for $E_1/E_2=8$ when compared to $E_1/E_2=4$. In the case of two-lane highway of 5.3m width, this increase is about 10%.



(a)

Figure 4.26: Lateral stress distribution of 9.6 m lane width at a depth of 0.1m for $E_1/E_2=4.0$ and 8.0

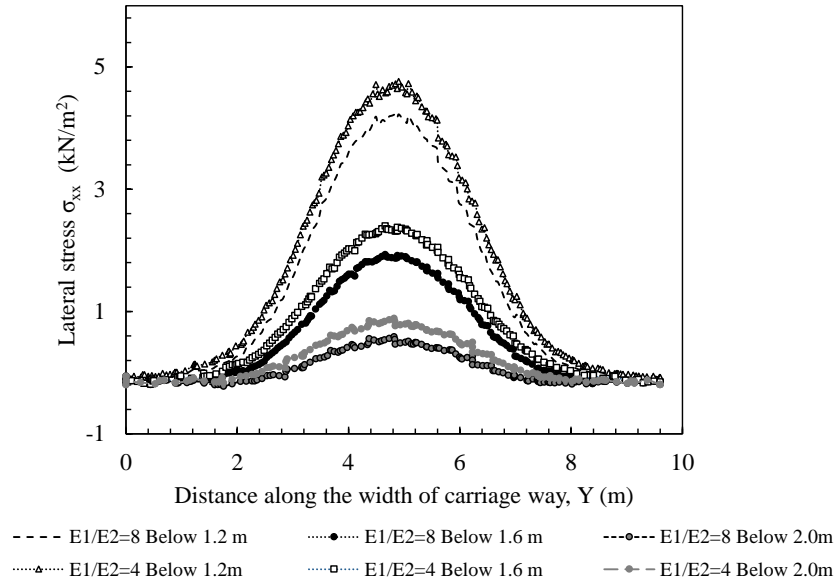
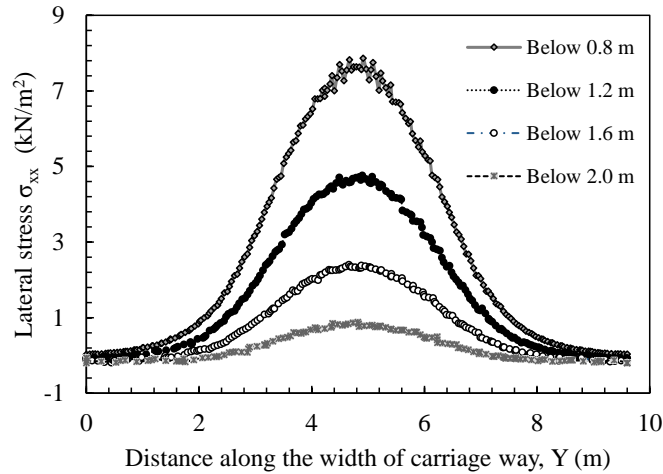


Figure 4.26: Lateral stress distribution of 9.6 m lane width at different depths of 1.2m, 1.6m and 2.0m for $E_1/E_2=4.0$ and 8.0

Figure 4.26(b) shows the variation of lateral stress with lane width of 9.6m at different depths of 1.2m, 1.6m 2.0m for $E_1/E_2=4.0$ and 8.0. Since, most of the developed stresses were dissipated within the top layer for $E_1/E_2=8$, the lateral stress are found to be lesser at different depths in the bottom layer compared to $E_1/E_2=4$.

4.8.3.3. Variation of lateral stress with depth for $E_1/E_2=4.0$

Figure 4.27 shows the variation of lateral stress with the width of carriageway at various depths for $D=0.175m$ and $E_1/E_2=4.0$ in the bottom layer. From Figures 4.19 and 4.21, it is observed that the lateral stresses produced for three-lane highway are lesser than that from two-lane highway. For instance, at a depth equal to 0.8m for $E_1/E_2=4$, the maximum lateral stress magnitude equal to about 7.6 kPa was observed for three-lane system, whereas for two lane highway, it was about 20 kPa.



**Figure 4.27: Lateral stress distribution of 9.6m lane width at different depth for $E_1/E_2=4$
For $z = 0.8\text{m}, 1.2\text{m}, 1.6\text{m}$ and 2.0m**

4.8.4 Four Lanes

Lane width was taken as 15m. As per IRC loading condition, two Class AA loads have to be considered for this lane width. Vehicle is symmetrically placed leaving minimum kerb distance on both the sides.

4.8.4.1. Variation of lateral stress with depth for $E_1/E_2=4.0$ and 8.0

Figure 4.28 shows that in the case of $E_1/E_2=8$, the average lateral stress at the surface of the top layer is 45% higher than that for $E_1/E_2=4.0$. Larger lateral stresses were noticed prominently at the top layer.

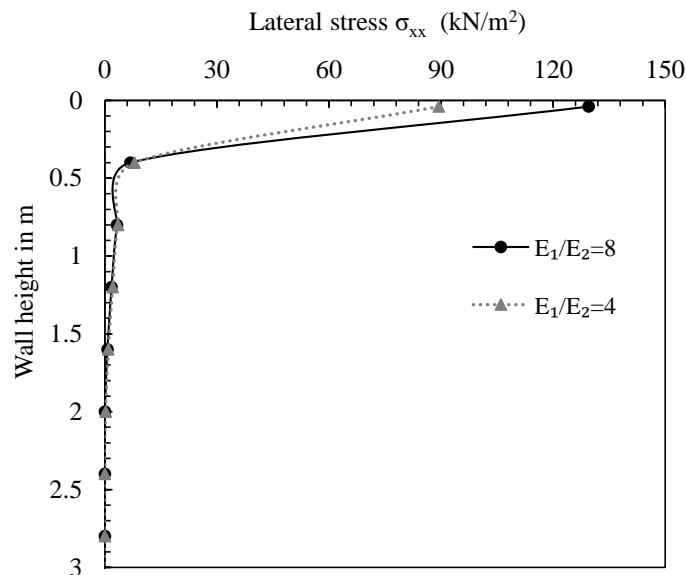


Figure 4.28: Average lateral stress distribution for $D=0.175$ For $E_1/E_2=4.0$ and 8.0

4.8.4.2. Variation of lateral stress with carriageway width for $E_1/E_2=4.0$ and 8.0

Figure 4.29 shows the variation of lateral stress with the width of carriageway of 15m for $E_1/E_2=4$ and 8 at a depth of 0.1m within the top stiff layer. For depths within the top layer, the lateral stresses

for $E_1/E_2=8$ produce higher values of stresses (about 30%) than that for $E_1/E_2=4$. In addition, most of the produced lateral stress was developed due to increase in E_1/E_2 is observed in the top layer.

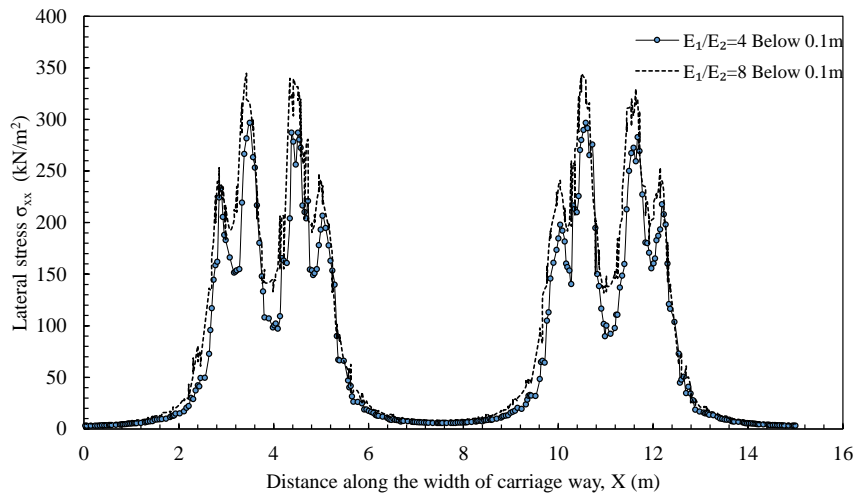


Figure 4.29: Lateral stress distribution of 15 m lane width at a depth of 0.1m for $E_1/E_2=4.0$ and 8.0

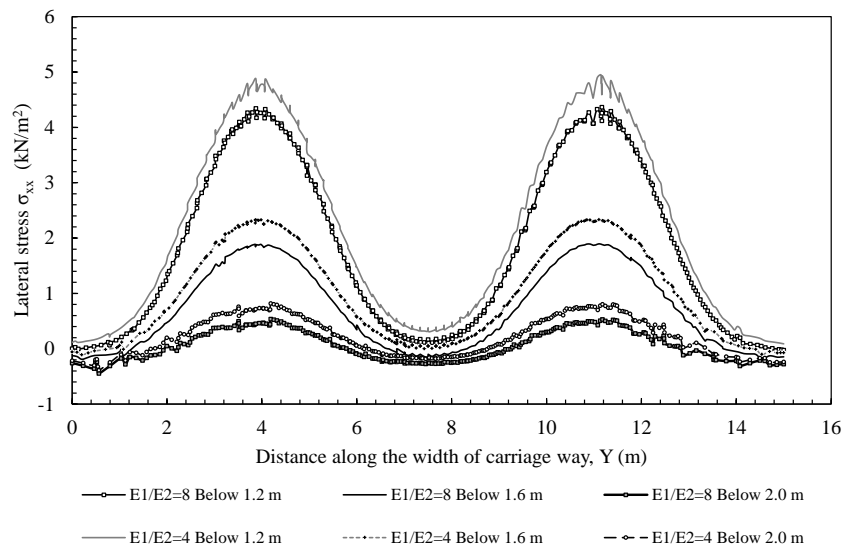


Figure 4.30: Lateral stress distribution of 15 m lane width at different depths of 1.2m, 1.6m and 2.0m for $E_1/E_2=4.0$ and 8.0

Figure 4.30 shows that for depths within the bottom layer, the lateral stresses for $E_1/E_2=4$ produce higher values of stresses (about 15%) than that for $E_1/E_2=8$. In addition, a decrease in maximum lateral stress due to increase in E_1/E_2 is observed in the bottom layer.

4.8.4.3. Variation of lateral stress with depth for $E_1/E_2=4.0$

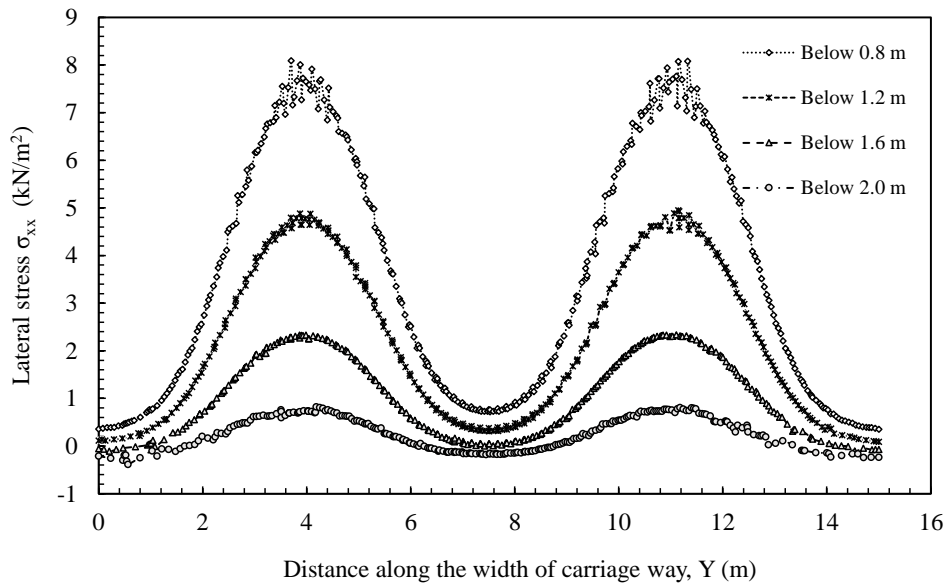


Figure 4.31: Lateral Stress distribution along lane width of 15m for $E_1/E_2=4.0$ at different depths of $z=0.8\text{m}$, 1.2m , 1.6m and 2.0m

Figure 4.31 shows that the vehicle produces maximum stress at the center of the each vehicle width and hence two peak values of lateral stresses can be seen. For depth more than about 2.0m, the bell-shaped distribution becomes flatter and the stress throughout the width shows almost a constant value.

4.8.5 Five Lane

Lane width was taken as 16.6m. Loading conditions are similar to four lanes. The vehicle is placed symmetrically about the center, hence the stress produced are also symmetrical about the center axis. Two peaks are observed at the center of each vehicle. Effect of moduli ratio along the depth and width was considered in the study.

4.8.5.1. Variation of lateral stress with depth for $E_1/E_2=4.0$ and 8.0

Figure 4.32 shows that the average lateral stress for $E_1/E_2=8$ is about 5% higher than that for $E_1/E_2=4$. The effect of moduli ratio is less pronounced in the case of five-lane highway.

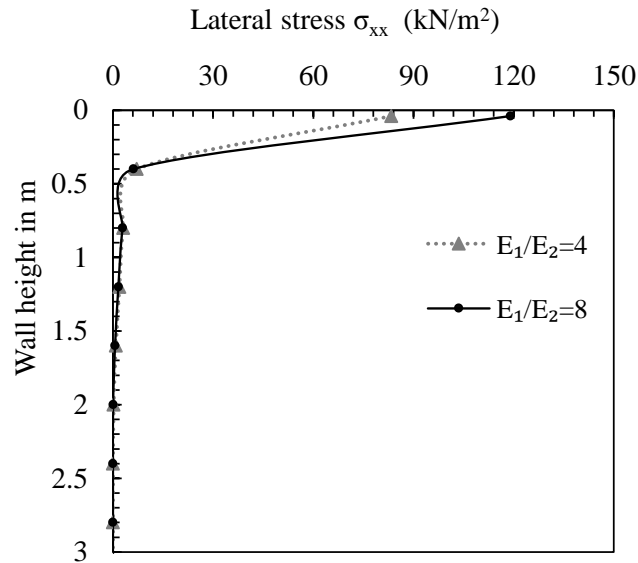


Figure 4.32: Average lateral stress distribution for $D=0.175\text{m}$ For $E_1/E_2=4.0$ and 8.0

4.8.5.2. Variation of lateral stress with carriageway width for $E_1/E_2=4.0$ and 8.0

Figure 4.33 also shows the effect of moduli ratio is less pronounced within the top layer for five-lane highway. The increase in the stress produced for $E_1/E_2=8$ compared to $E_1/E_2=4$ is about 4%, which is lesser compared to the increase observed from two-lane to four-lane (which was between 10% to 45%).

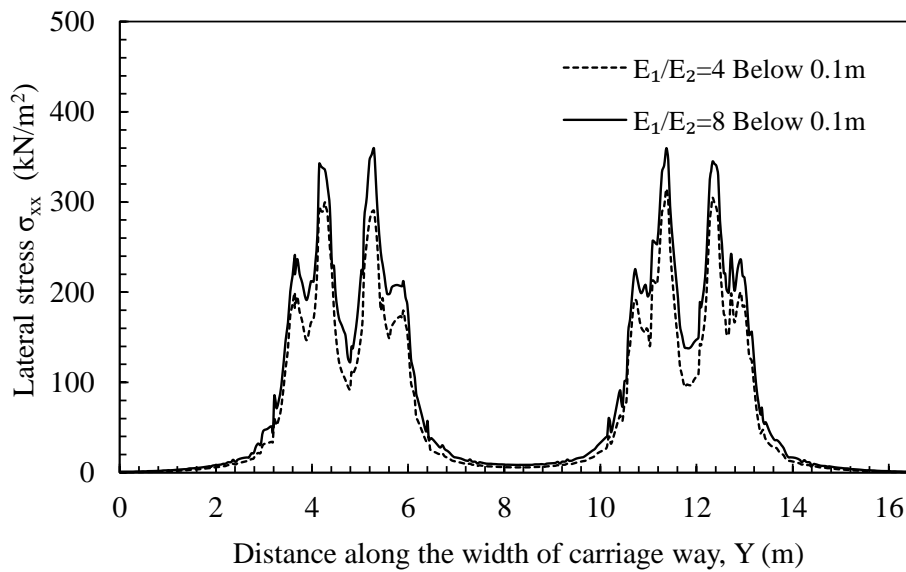


Figure 4.33: Lateral stress along the lane width of 16.6m for $E_1/E_2=4.0$ and 8.0 at a depth of $z=0.1\text{m}$

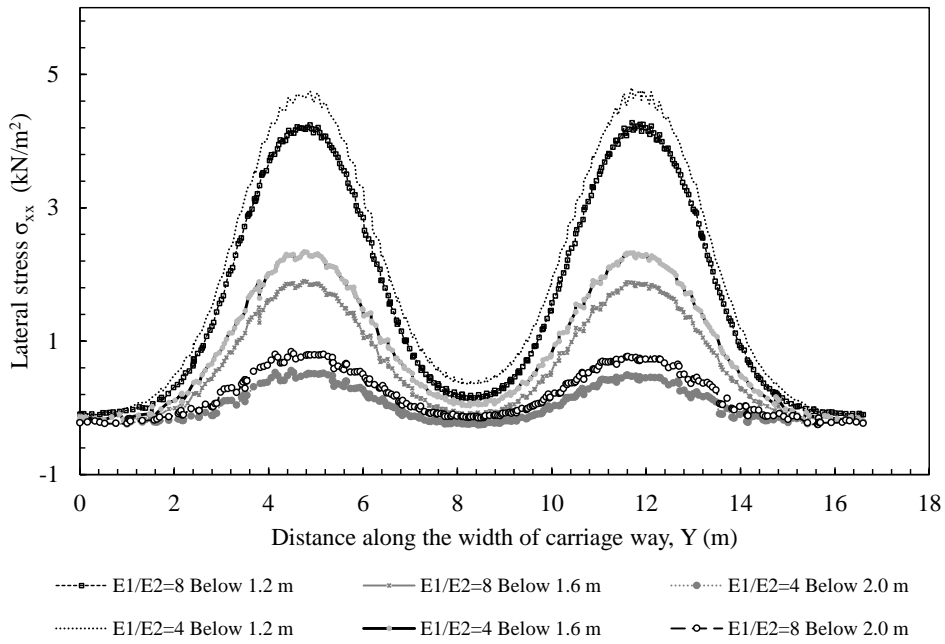


Figure 4.34: Lateral stress along the lane width of 16.6m for $E_1/E_2=4.0$ and 8.0 at different depths of $z=1.2\text{m}$, 1.6m and 2.0m

Figure 4.34 shows the effect of moduli ratio on abutment wall for a five-lane highway considered in the study. The effect of moduli ratio is more noticeable at higher depths. For example, at 1.2m depth, the increase in lateral stress for $E_1/E_2=4$ is about 7.6% compared to that for $E_1/E_2=8$. At 1.6m depth, this increase is about 19%.

4.8.5.3. Variation of lateral stress with depth for $E_1/E_2=4.0$

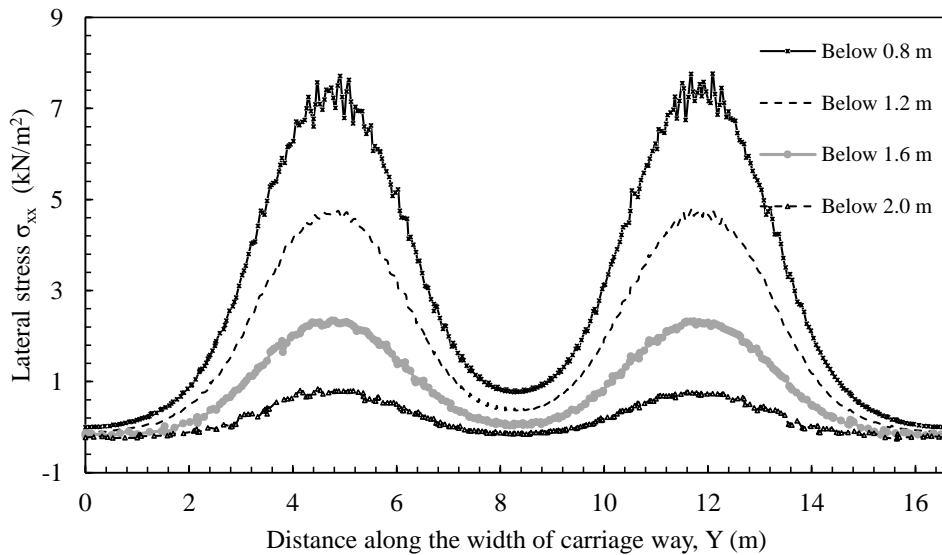


Figure 4.35: Lateral Stress along width of 16.6m for $E_1/E_2=4.0$ at different depths of $z=0.8\text{m}$, 1.2m , 1.6m and 2.0m

Figure 4.35 shows the variation of lateral stress distribution for $E_1/E_2=4.0$ at different depths in the bottom layer.

4.9 Lateral stress distribution considering Three-layered system

The purpose of the approach slab is to minimize the effects of differential settlement between the bridge abutment and the embankment fill, to provide a smooth transition between the pavement and the bridge, to prevent voids that may occur under the slab and to provide a better seal against water percolation and erosion of the backfill material. In the present study, three-layered system with an approach slab over the granular base layer resting on the embankment fill material was considered. Insufficient length of approach slabs can create differential settlements at the bridge end. However, lengths varied from 5m to 10m and thicknesses ranged from 230mm to 430mm performed well in the study by Hoppe (1999). As per MORTH report on wearing coat and appurtenances, minimum length of approach slab is 3.5m and minimum thickness of approach slab is 300mm. In the present study, an approach slab of length 6.0m and thickness of 0.25m is considered overlying the granular base resting on the embankment fill.

4.9.1 Single lane

Lane width of 3.8m is considered for single lane Highway Bridge in the study. Approach slab is provided in connection with abutment and granular base layer. In PLAXIS, approach slab is modeled as plate element with Young's modulus 22GPa. E_0 is Young's modulus of approach slab, E_1 is deformation modulus of granular base course and E_2 is deformation modulus of embankment fill material. Poisson ratio for approach slab is taken as 0.15. IRC Class A loading is used for the corresponding lane width.

4.9.1.1. Comparison of Variation of lateral stress with depth for $E_1/E_2=8.0$

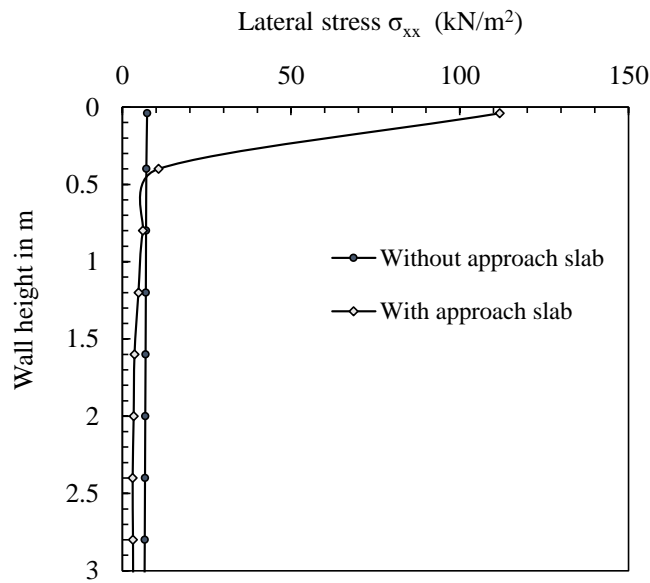


Figure 4.36: Lateral stress distribution for lane width of 3.8m with approach slab and without approach slab for $E_1/E_2=8$

Figure 4.36 shows the average lateral stress variation when there is an approach slab placed over the granular base course as explained in the earlier section. With approach slab, the distribution of lateral stress is almost uniform along the wall height. The lateral stress produced along the height of the wall is relatively small due to very stiff slab placed at the top.

4.9.1.2. Variation of lateral stress with carriageway width for $E_1/E_2=8.0$

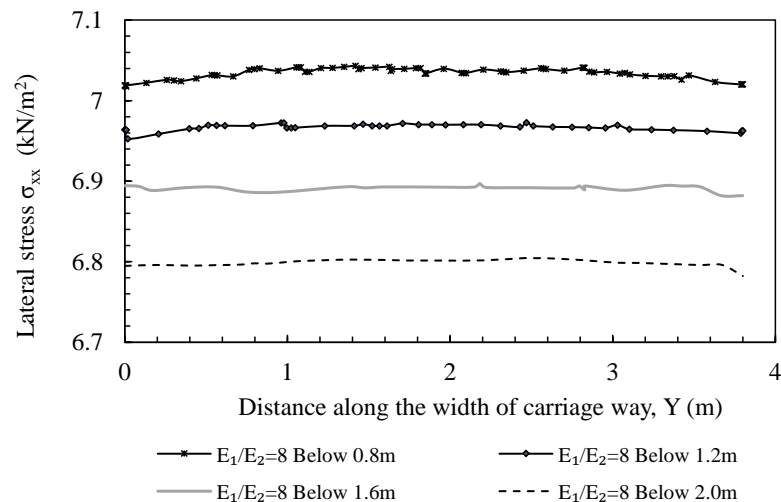


Figure 4.37: Lateral stress distribution along the width of carriageway of 3.8m for $E_1/E_2=8$ at different depths of $z=0.8m, 1.2m, 1.6m$ and $2.0m$ with approach slab

Figure 4.37 shows lateral stress developed at different depths for $E_1/E_2=8$. It is found that stress distribution is uniform along the width unless in a bell shape which is due to approach slab on top. As discussed in the previous section, the stresses are uniform along the depth. Hence, the stress difference between two depths say 0.8m and 1.2m is about 0.1kPa.

4.9.2 Two lanes

Lane width is between 5.3 and 7.0m and the results are shown for lane width equal to 5.3m is provided in this section. IRC Class AA loading is adopted in the analysis. Moduli ratio of approach slab to granular base layer is about 90 in the study. Studies on the $E_1/E_2=4.0$ and 8.0 are explained in the subsequent section.

4.9.2.1. Comparison of Variation of lateral stress with depth for $E_1/E_2=8.0$

Figure 4.38 shows the variation of lateral stress on abutment with and without an approach slab. With an approach slab, the lateral stress distribution is relatively small compared to that without an approach slab. Hence, providing an approach slab reduces differential settlement as well as lateral stress on the abutment.

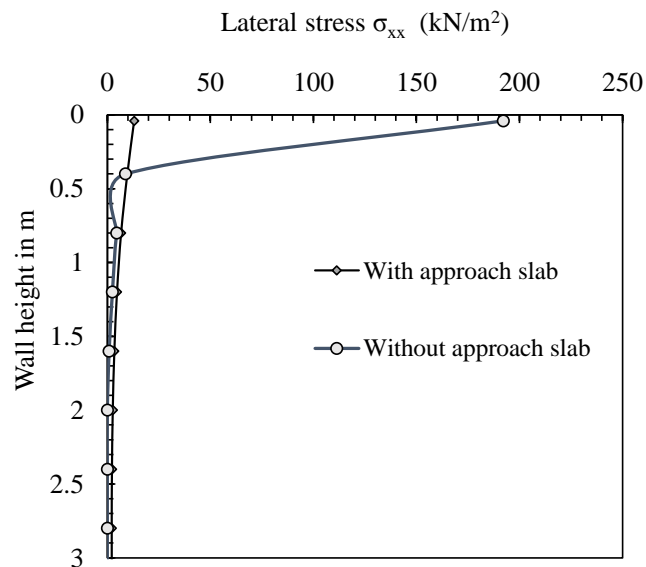


Figure 4.38: Lateral stress distribution for lane width of 5.3m with approach slab and without approach slab for $E_1/E_2=8$

4.9.2.2. Variation of lateral stress with carriageway width for $E_1/E_2=8.0$

Figure 4.39 shows the variation of lateral stress along the width of 5.3m for $E_1/E_2=8.0$ at different depths of $z=0.8$ m to 2.0m. The lateral stress observed is less than 10kPa below 0.4m of wall height.

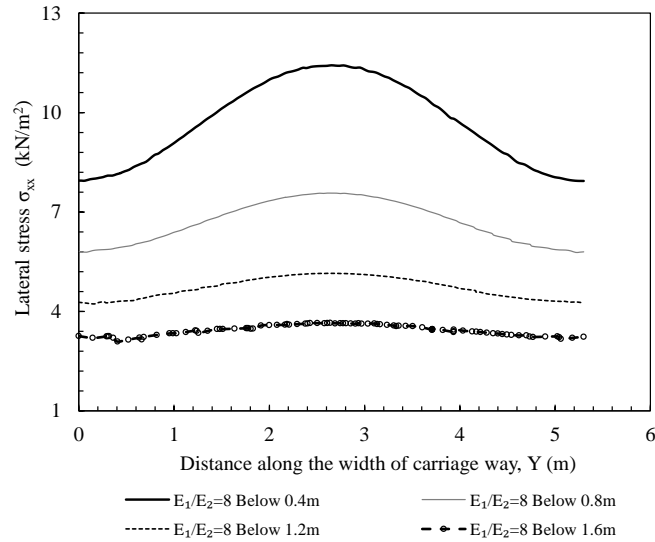


Figure 4.39: Lateral stress distribution along the width of carriageway of 5.3m for $E_1/E_2=8$ at different depths of $z=0.4\text{m}$, 0.8m , 1.2m and 1.6m with approach slab

4.9.3 Three lanes

Lane width is 9.6m is taken as three lane Highway Bridge. The results of lateral stress distribution is compared with the results of lateral stress distribution without approach slab for $E_1/E_2=8.0$.

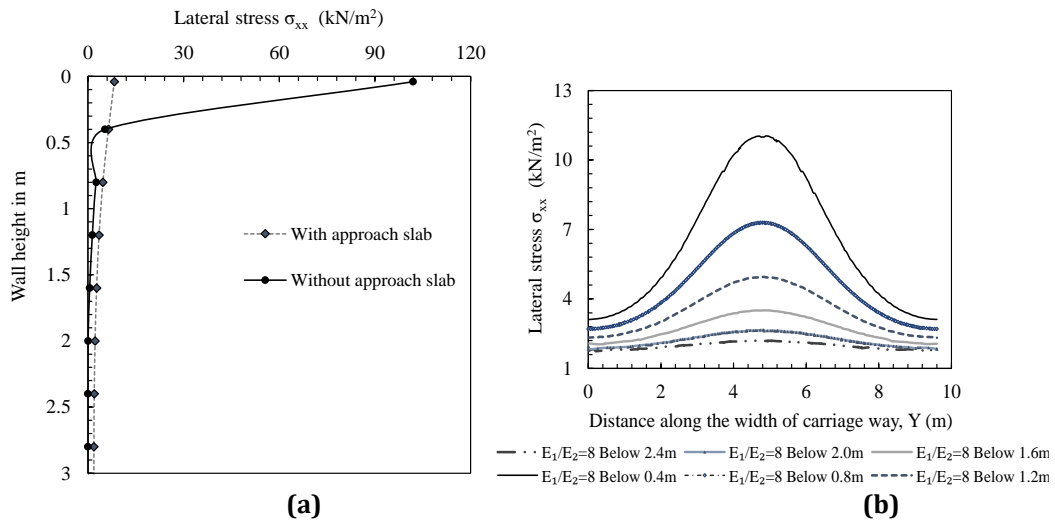


Figure 4.40: Lateral stress distribution for lane width of 9.6m for $E_1/E_2=8$ (a) Along the height with approach slab and without approach slab (b) along the width of carriageway at different depths of $z=0.4\text{m}$, 0.8m , 1.2m , 1.6m , 2.0m and 2.4m with approach slab

Figure 4.40(a) shows the variation of lateral stress distribution for $E_1/E_2=8$. For instance, with approach slab the average lateral stresses developed are very minimum compared to that the stresses produced for without approach slab. As shown in Figure 4.40(b), the maximum lateral stresses reduce with depth and it is reduced to one-half at each 0.4m increment of depth.

4.9.4 Four lanes

Lane width considered for four lane highway is 15.0m. As per IRC6-2000, two lanes of IRC Class AA loading is used. Figure 4.41(a) shows the variation of lateral stress calculated from numerical results for both considering with approach slab and without approach slab for $E_1/E_2=8.0$. Lateral stress distribution is found to be relatively small and the variation of stress is uniform in the bottom layer. Figure 4.41(b) shows two maxima are formed symmetrically corresponding to the center of each vehicle. At depth of 2.4m, lateral stresses are almost reached a constant value.

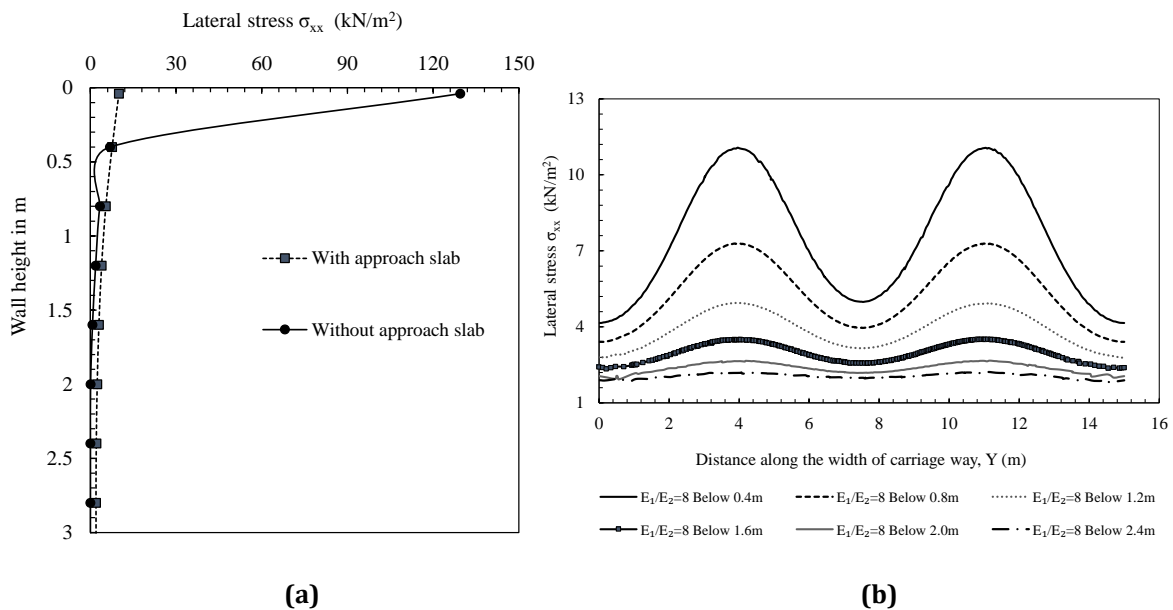
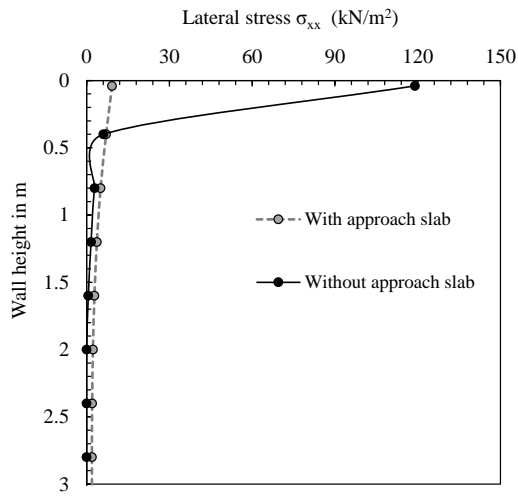


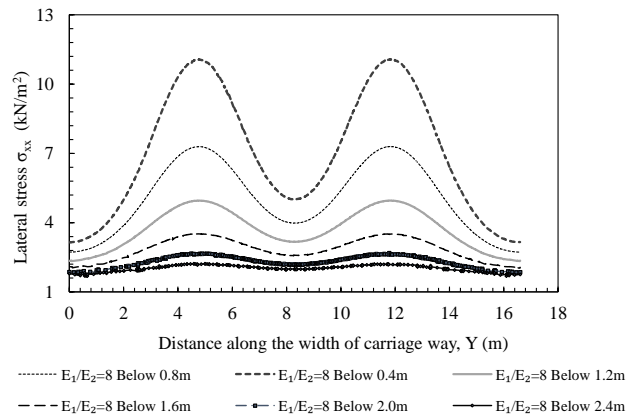
Figure 4.41: Lateral stress distribution for lane width of 15m for $E_1/E_2=8$ (a) along the height with approach slab and without approach slab, and (b) along the width of carriageway at different depths of $z=0.4\text{m}$, 0.8m , 1.2m , 1.6m , 2.0m and 2.4m with approach slab

4.9.5 Five lanes

Lane width considered for five-lane Highway Bridge is 16.6m. Two lanes of IRC Class AA loading is used as per IRC 6-2000. Figure 4.42(a) shows the variation of average lateral stress on abutment, lesser lateral stress at the top were noticed, unlike for the case when no approach slab was used. Due to less the stresses at the top, the moment produced at the base will also get reduced which reduce the effect of live loading on abutment. Figure 4.42(b) shows the variation along the width of the carriageway for $E_1/E_2=8.0$. It is also learned that in presence of approach slab the effect of E_1/E_2 is not noticeable in the case of three-layered system.



(a)



(b)

Figure 4.42: Lateral stress distribution for lane width of 16.6m for $E_1/E_2=8$ (a) along the height with approach slab and without approach slab, and (b) along the width of carriageway at different depths of $z=0.4\text{m}$, 0.8m , 1.2m , 1.6m , 2.0m and 2.4m with approach slab

Chapter 5

Equivalent surcharge for live loads on Abutments

5.1 Introduction

Determination of the equivalent height of surcharge to calculate the lateral stress on abutments due to vehicular loads will be useful in the design of abutments. This chapter describes briefly about the equivalent height of surcharge for various lane widths (single lane to five lane highways). Two models were considered and explained in detail in the subsequent sections. The calculation procedure followed in determining the equivalent heights are explained in Section 5.3.

5.2 Two-Layered System-Model I

The finite element model consists of two-layered soil system. The top layer of 0.3m thickness consists of granular base course with the properties given in Table 5.1. Abutment wall height is 6m. Bottom layer of 5.7m is made of embankment backfill. Linear elastic analysis was adopted. Typical range of material properties considered in the study is provided in Table 5.1.

Table 5.1: Properties of the material layers considered for Model I

Layer	Deformation modulus, E (Range adopted) (MPa)	Representative Deformation modulus, E (MPa)	Poisson ratio, ν
Granular Base Layer	250-260	240	0.3
Embankment Backfill	30-60	30-60	0.3

5.3 Calculation of Equivalent height of surcharge

The procedure adopted to calculate the equivalent heights were explained earlier in the previous chapter. Section 5.3.1 explains an example calculation for two lane of 5.3 m width and for moduli ratio of 4. Parametric Study was carried out by two different methods: (a) Equivalent moment method, and (b) Equivalent force method. Both the methods are explained briefly in the following section.

5.3.1 Equivalent bending moment method

Table 5.2 shows the procedure of calculation of equivalent surcharge for a two-lane case with $E_1/E_2=4.0$. The average uniform lateral stress calculated at each 0.4 m increment of wall is given and the moment is calculated with the formula given in equation [1]. The moment due an equivalent height of surcharge, h_{eq} , is calculated using equation [2]. Equating the moment from Equations [1] and [2] gives the equivalent surcharge height.

$$M_E = z \sum_{i=1}^n \beta \sigma_i - \sum_{i=1}^n d_i \beta \sigma_i \quad (1)$$

$$M_c = \frac{1}{2} K \gamma h_{eq} H^2 \quad (2)$$

Table 5.2: Procedure to determine the bending moment from the numerical results for lane width of 5.3m for $E_1/E_2=4.0$

Depth (m)	σ_i (kPa)	$(\sigma_i)_{avg}$ (kN/m)	β (m)	$\beta * \sigma_i$ (kN)	d_i (m)	$\beta * \sigma_i * d_i$ (kN.m)
0.04	111.25	61.72	0.36	22.22	0.20	4.44
0.40	12.19	10.87	0.40	4.35	0.60	2.61
0.80	9.55	7.95	0.40	3.18	1.00	3.18
1.20	6.35	5.15	0.40	2.06	1.40	2.89
1.60	3.95	3.27	0.40	1.31	1.80	2.35
2.00	2.58	2.26	0.40	0.90	2.20	1.98
2.40	1.93	1.83	0.40	0.73	2.60	1.90
2.80	1.72	1.95	0.40	0.78	3.00	2.34
3.20	2.17	2.29	0.40	0.92	3.40	3.12
3.60	2.41	2.84	0.40	1.14	3.80	4.32
4.00	3.27	3.82	0.40	1.53	4.20	6.42
4.40	4.37	5.08	0.40	2.03	4.60	9.35
4.80	5.80	6.62	0.40	2.65	5.00	13.24
5.20	7.44	8.68	0.40	3.47	5.40	18.75
5.60	9.92	11.52	0.40	4.61	5.80	26.73
6.00	13.12					

5.3.2 Equivalent force method

Similar procedure is followed using equivalent force method wherein the total force was calculated by summing up the force from numerical results at each wall increment. The total force due to equivalent height of surcharge, h_{eq} , is calculated from equation [3].

$$F_c = K\gamma h_{eq} H \quad (3)$$

Total force at each 0.4m increment from numerical results for lane width of 5.3m for $E_1/E_2=4.0$ are given in Table 5.3. Equating the total force from Equation [3] and numerical integration gives the equivalent height of surcharge.

Table 5.3: Procedure to determine the total force from the numerical results for lane width of 5.3m for $E_1/E_2=4.0$

Depth (m)	σ_i (kPa)	$(\sigma_i)_{avg}$ (kN/m)	β (m)	$\beta^*\sigma_i$ (kN)
0.04	111.25	61.72	0.36	22.22
0.40	12.19	10.87	0.40	4.35
0.80	9.55	7.95	0.40	3.18
1.20	6.35	5.15	0.40	2.06
1.60	3.95	3.27	0.40	1.31
2.00	2.58	2.26	0.40	0.90
2.40	1.93	1.83	0.40	0.73
2.80	1.72	1.95	0.40	0.78
3.20	2.17	2.29	0.40	0.92
3.60	2.41	2.84	0.40	1.14
4.00	3.27	3.82	0.40	1.53
4.40	4.37	5.08	0.40	2.03
4.80	5.80	6.62	0.40	2.65
5.20	7.44	8.68	0.40	3.47
5.60	9.92	11.52	0.40	4.61
6.00	13.12			

5.4 Critical position of the vehicle

To determine the critical effect of distance of vehicle from the back of wall, analysis was carried out for the lane width of 5.3m and 13.2m for $E_1/E_2=4$, and the values are tabulated in Table 5.4. Similar to the observation from the lateral stress distribution, $D=0.175m$ shows a maximum equivalent surcharge results.

Table 5.4: Equivalent height of surcharge determined using Equivalent moment method for $E_1/E_2=4$

Lane width (m)	Distance from the back of abutment wall to the center of front wheel, D (m)						
	0.175	0.265	0.350	0.525	0.700	0.875	0.965
5.3	1.305	1.030	0.826	0.710	0.793	0.812	0.815
13.2	1.035	0.845	0.680	0.577	0.642	0.650	0.651

It can be seen that increase in the distance from the wall results in decrease in the value of h_{eq} . After a distance of 0.525m, there is an increase in the equivalent surcharge. The change in h_{eq} is not significant beyond a distance of 0.700m in the case of both 5.3m and 13.2m lane widths.

5.5 Effect of Moduli Ratio

Referring to Tables 5.4 and 5.5, the equivalent surcharge values determined from equivalent bending moment method gives higher values than that compared to equivalent force method. For instance, considering a lane width equal to 5.3m, the equivalent height of surcharge from bending moment method is found to be 60% higher than that from force method. Two-lane carriageway of width 5.3m gives 0.819m and this value for four-lane carriageway of 13.2 m width would be 0.668m, which is about 23% lesser than that for two lanes. It can also be concluded that the increase in the lane width reduces the effect of surcharge load. In addition, the higher the lane width, the lower the equivalent surcharge that needs to be considered.

Table 5.5: Equivalent height of surcharge determined using Equivalent Force method for $E_1/E_2=4$

Lane width (m)	Distance from the back of abutment wall to the center of front wheel, D (m)						
	0.175	0.265	0.350	0.525	0.700	0.875	0.965
5.3	0.819	0.704	0.610	0.579	0.641	0.671	0.682
13.2	0.668	0.576	0.500	0.466	0.530	0.540	0.546

As stated in the previous analysis for the 2D case, the lateral stresses are higher at the top layer for higher moduli ratio. Higher lateral stresses produce larger bending moment about the base. This can be observed in the results of increased equivalent height for higher moduli ratio. For instance, four-lane carriageway of 13.2m width shows increase in the h_{eq} value. It is about 22% for $E_1/E_2=4$ from $E_1/E_2=8$ for $D=0.175$ m. From Table 5.6 and Table 5.7, it was inferred that for vehicle distance $D=0.7$ m and more, equivalent surcharge is almost uniform regardless of the lane width or the moduli ratio.

Table 5.6: Equivalent height of surcharge determined using Equivalent moment method for $E_1/E_2=8$

Lane width (m)	Distance from the back of abutment wall to the center of front wheel, D (m)						
	0.175	0.265	0.350	0.525	0.700	0.875	0.965
5.3	1.736	1.274	0.953	0.616	0.710	0.751	0.765
13.2	1.333	1.032	0.766	0.504	0.565	0.606	0.613

Table 5.7: Equivalent height of surcharge determined using Equivalent force method for $E_1/E_2=8$

Lane width (m)	Distance from the back of abutment wall to the center of front wheel, D (m)						
	0.175	0.265	0.350	0.525	0.700	0.875	0.965
5.3	1.057	0.826	0.670	0.519	0.591	0.631	0.649
13.2	0.813	0.669	0.539	0.422	0.470	0.507	0.519

5.6 Values of equivalent height

Table 5.8 gives the values of h_{eq} for lane widths ranging from 3.8m to 16.6m using both equivalent moment and force methods. Single lane gives a value around 0.7m. For two lane it is about 1.305m, which is 1.9 times higher than that for single lane. Lane widths equal to 5.3m and 7.0m are designed as two lanes. It can be inferred that the equivalent surcharge intensity decreases with the increase in the lane width. Sufficient increase in the lane width reduces the effect of stresses on the abutment wall. It is determined that the percentage difference in the equivalent surcharge is about 33% for lane width 7.0m than that compared to 5.3m.

Table 5.8: Values of Equivalent height of surcharge, h_{eq} for different lane widths for $E_1/E_2=4$ for Model I

Lane width (m)	h_{eq} (m)	
	Equivalent moment method	Equivalent force method
3.8	0.700	0.699
5.3	1.305	0.819
7.0	0.981	0.631
9.6	0.729	0.467
13.2	1.035	0.668
15	0.921	0.592
16.6	0.848	0.543

The equivalent surcharge height considered in the current IRC practice is about 1.2m, which need not be enforced for all the lane widths. The critical equivalent height of surcharge observed from the study is about 1.305m. Minimum lane width equal to 5.3m has higher effect due to lateral stress on abutment and hence it can be suggested that in order to reduce the lateral stresses on the abutment, the lane width for two lanes could be around 7.0m. Similarly, for four lanes the lane width could be more than 13.2m.

Values of h_{eq} for different lane widths for $E_1/E_2=8$ are given in Table 5.9. For $E_1/E_2=8$, the equivalent height of surcharge varies from 0.7m-to-1.7m. The values are higher than for $E_1/E_2=4$. As explained

in section 5.2, the deformation modulus of bottom layer is 60kPa and the granular base course layer is 240kPa, gives a moduli ratio of 4. The increase may be due to less stiff bottom layer in the case of moduli ratio equal to 8. It can be suggested to have higher lane widths and good quality of backfill to reduce the influence of lateral stresses on abutment wall.

Table 5.9: Values of Equivalent height of surcharge, h_{eq} for different lane widths for $E_1/E_2=8$ for Model I

Lane width (m)	h_{eq} (m)	
	Equivalent moment method	Equivalent force method
3.8	0.737	0.720
5.3	1.736	1.057
7.0	1.266	0.776
9.6	0.937	0.573
13.2	1.333	0.813
15	1.192	0.730
16.6	1.089	0.666

5.7 Three-Layered System-Model-II

An approach slab of 0.25m thickness and 6 m length was considered at the transition between abutment and the approach road. The properties of approach slab and other soil layers considered are as given in Table 5.10. In PLAXIS, plate elements are used to model approach slab. E_o is the deformation modulus of approach slab.

Table 5.10: Properties of the material layers considered in Model II

Layer	Deformation modulus, E (MPa)	Poisson ratio, ν
Approach slab	22×10^3	0.15
Granular Base layer	240	0.3
Embankment Backfill	30-60	0.3

Table 5.11, lists the values of h_{eq} for different lane widths for $E_1/E_2=4$. In the case of Model II (i.e., with an approach slab in the model), the equivalent heights of surcharge are found to give lesser values compared to the one without approach slab. For 5.3 m lane width, the value of h_{eq} is almost reduced to half. Advantages of having approach slab can be well understood from the results.

Table 5.11: Equivalent height of surcharge determined for Model II using Equivalent moment method for

Lane width (m)	$E_1/E_2=4$	
	h_{eq} (m)	
	Equivalent moment method	Equivalent force method
3.8	0.880	0.885
5.3	0.645	0.611
7.0	0.548	0.520
9.6	0.466	0.444
13.2	0.615	0.578
15	0.527	0.502
16.6	0.5	0.477

The values of equivalent heights of surcharge range from 0.5 to 0.9m. Table 5.12 indicates the effect of the modulus of the granular base course is less pronounced when there is an approach slab. In the case of approach slab, the effect of moduli ratio ($E_1/E_2=4$ and 8) on lateral stresses is negligible. For lane width of 7.0m, the percentage difference between moduli ratio 4 and 8 is about 0.5%. Similarly results were observed for other cases of lane widths. The effect of E_1/E_2 is less pronounced because of the approach slab placed on top.

Table 5.12: Equivalent height of surcharge determined for model II using Equivalent moment method for

Lane width (m)	$E_1/E_2=8$	
	h_{eq} (m)	
	Equivalent moment method	Equivalent force method
3.8	0.880	0.885
5.3	0.643	0.622
7.0	0.545	0.529
9.6	0.463	0.449
13.2	0.602	0.577
15	0.525	0.509
16.6	0.498	0.484

Chapter 6

Conclusions

In this study, the actual stress distribution on bridge abutment due to live loads (wheel loads) was obtained using Finite element package PLAXIS 2D and PLAXIS 3D. A Two-dimensional model was developed using PLAXIS 2D and has been validated with the available elastic solutions.

- The Finite element model in PLAXIS 2D is validated by comparing the stresses produced due to strip loading on abutment in homogeneous medium with that of the elastic solution proposed by Scott (1963).
- Vertical Stress distribution in a two-layered system obtained from PLAXIS 2D is validated with the solutions for two-layered system by Burmister (1943) using strain continuity equations.
- In a three-layered system, interface radial and vertical stresses obtained at each layer interface from the FE model is compared with the results by Jones (1962).

An abutment-Soil system was modeled as a two-layered system with stiffer top layer which represents the pavement or the granular layer placed over the embankment fill. A Parametric study was conducted to study the effect of moduli ratio of the two layers by varying the E_1/E_2 ratio from 1-to-10 and the effect of the thickness of the top layer by varying the thickness-to-radius ratio from 0.25-to-0.5 in the stress distribution on abutment.

From the parametric study the following conclusions are drawn:

- For thickness of the top layer equal to 0.5m, an increase in the E_1/E_2 ratio reduces the vertical stress in the soil medium. At the interface of the two-layer, the vertical stress is about 86% of the applied stress for $E_1/E_2=10$. However, in a homogeneous medium (i.e., $E_1/E_2=1.0$), the interface vertical stress is about 100%. Reduction in the vertical stress is more significant for $E_1/E_2=10$.
- It may be noticed that when the stiffer layer is present on the top of the softer layer, the stress dissipation occurs faster in the top layer. For $E_1/E_2=5$, an increase in the thickness of top layer, produces lesser vertical stress in the fill material.

- Influence of moduli ratio on lateral stress is significant in the top layer. Higher moduli ratio produces larger lateral stress in the top layer. Similarly, as the thickness of the top layer increases, there is a significant increase in the lateral stress in the upper layer.
- Increase in the E_1/E_2 ratio and the top layer thickness reduces the settlement.

Three-dimensional model was developed using PLAXIS 3D. Finite element model was validated for a plane strain condition with the available solution from PLAXIS 2D which validated the appropriateness of the element size and meshing of the 3D-model. An abutment-Soil system was modeled for two cases: (i) two-layered system where the GSB/Approach slab is placed over the embankment fill material and (ii) three-layered system where approach slab with sufficient length was placed over the GSB underlying embankment fill material.

Case (I): Two-layered system

- The lateral stresses shows bell-shaped variation and the bell-shaped nature reduces with the increase in depth.
- Lateral stress within the top stiff layer produces higher stresses when $E_1/E_2=8.0$ which is due to the fact that most of the stresses will be dissipated in the stiff layer.
- In the case of $E_1/E_2=4$, at any depth in the bottom layer the lateral stress developed is larger compared to that of $E_1/E_2=8$. This can be explained by the theory of two-layered system where higher the moduli ratio, the stresses will be taken care at the top layer. Hence, lower the stresses developed at the bottom layer.
- Lane widths from 3.8m to 15.0m shows an increase in the average lateral stress for $E_1/E_2=8$, it is about 30-45% higher than that of $E_1/E_2=4$ at the surface of top layer.
- Lane width of 16.6m shows an increase in the average lateral stress for $E_1/E_2=8$, it is about 5% higher than that of $E_1/E_2=4$ at the surface of top layer.

Case (II): Three-layered system

- Average lateral stresses produced are very minimal when compared with the two-layered system. This may be due to the presence of very stiff approach slab.
- Presence of approach slab is not only important in reducing the differential settlement problem, but also to take up higher stress and transfer very less lateral stress to the bottom layers.
- Effect of E_1/E_2 is negligible when approach slab is present on top.

Equivalent height of surcharge

- Equivalent heights of surcharge values determined from equivalent bending moment method gives higher values compared to equivalent force method.
- Increase in the lane width reduces the effect of surcharge load on stress, meaning higher the lane width, the lower the equivalent surcharge.

- The equivalent surcharge height considered in the current IRC practice is about 1.2m which need not to be enforced for all the lane widths.
- The critical equivalent height of surcharge obtained from the study for Case (I) two-layered system is about 1.305m. Minimum lane width equal to 5.3m gives higher lateral stress on abutment and hence it can be suggested that the lane width for two lanes be around 7.0m to reduce the lateral stresses. Similarly, four lanes the safest lane width can be more than 13.2m.
- For case (II) three-layered system, the values of equivalent height of surcharge range from 0.5 to 0.9m for various lane widths.
- Equivalent heights of surcharge are recommended for different lane widths and for different moduli ratios for two-layered and three-layered systems.

References

- [1] Jones, A. (1962). "Tables of stresses in three layer Elastic system." Highway Research Board-Bulletin 342, pp. 176-214
- [2] Peattie, K.R. (1962). "Stresses And strain Factors For Three layer Elastic System", HRB-Bulletin 342, pp. 315-353
- [3] Poulos, H.G. & Davis, E.H. (1974) "Elastic solutions for soil and rock mechanics"
- [4] Standard specifications and code of practice for road bridges Indian Road Congress 6 (2000), section II.
- [5] Magdy A. Zahw et al. (2012). "Evaluation of highway concrete Bridge approach slabs." International journal of Advanced science and Engineering Technology, Vol.2, No.1, pp.52-57
- [6] Kim, J. and Barker, R. (2002). "Effect of Live Load Surcharge on Retaining walls and Abutments." Journal of Geotechnical Geo-environmental Engineering, Vol.128, No.10, pp.803-813
- [7] Christie et al.(2010) "Development of Traffic surcharge models for Highway structures", ICE proceedings, Bridge Design to Eurocodes: UK Implementation
- [8] Spangler, M.G. and Mickle, L. (1956) "Lateral earth pressure on retaining walls due to backfill surface loads." Unpublished thesis, IOWA state college
- [9] Akbulut, H and Aslantas, K. (2005). "Finite element analysis of stress distribution on bituminous pavement and failure mechanism." Journal of Materials and Design, Vol.26, pp.383–387
- [10] Burmister, D.M. (1945). "The general theory of stresses and displacements in layered systems I", Journal of applied physics, Vol.16, pp.89
- [11] Bowles, J.E (1996), "Foundation analysis and design", 5th ed., McGraw Hill, New York, NY, USA.
- [12] Burmister, D.M. (1943). "The Theory of stresses and displacements in layered systems and applications to design of Airport Runways", Highway research Board, Vol.23, pp.126
- [13] Nagendra Prasad and Manohara Reddy. (2012) "A Simple approach to Analysis of stresses in Two layered Soil Medium for Engineering Applications", International Journal of Earth sciences and Engineering, Vol.5, No.6, pp.01
- [14] Chapter-12, Bridge manual of Wiscosin DOT

- [15] Terzaghi, K., Peck, R. B., and Desri, G. (1996). "Soil mechanics in engineering practice", 3rd Ed., Wiley, New York.
- [16] Peck R. B., Hanson, W.E., and Thornburn T.H. (1974). "Foundation engineering", 2nd Ed., Wiley, New York.
- [17] Ersan Yildiz (2003). "Lateral Pressures on Rigid Retaining Walls, A Neural Network Approach" Master thesis submitted to the Middle East Technical University.
- [18] Brinkgreve et al.(2011) Manual for Plaxis 3D-2011
- [19] Brinkgreve et al.(2011) Manual for Plaxis 2D-2011
- [20] Spangler M.G., and Handy L.R., "Soil Engineering", 4th Edition. Harper and Row, New York.